

Los sistemas policultivo previenen la propagación fitopatógenos

Dr. Jhony Eredi Ramírez Cancino

jhony.ramirezcanino@viep.com.mx

Centro de Agroecología, Instituto de Ciencias, Benemérita Universidad Autónoma de Puebla

Phytophthora es una familia de fitopatógenos de gran trascendencia ecológica debido a la vasta variedad de plantas a las que puede atacar (silvestres y de interés comercial). Por ejemplo, *Phytophthora Capsici*, ataca a una amplia gama de especies alimenticias, como la papa, jitomate y chile. En 2014, en el país se reportaron grandes pérdidas económicas debido a las afectaciones de *P. Capsici* en plantaciones de chile. En la región de San Martín Texmelucan, se reportan pérdidas entre el 90% y 100% de las plantaciones de chile chilaca y poblano. En la región de Tehuacán, *Phytophthora* merma la producción de amaranto y chíá. Similarmente, la región de Atlixco es sumamente afectada por *P. Cinnamomi*, responsable de la enfermedad conocida como la tristeza del aguacatero, provocando la muerte de miles de árboles. Además de las consecuencias económicas provocadas por el bajo rendimiento de la plantación y la mala calidad de los productos, se propicia la reducción de la superficie productora y la sustitución o abandono de los cultivos. Por sus características fisiológicas particulares, no existen tratamientos químicos eficaces para el control de *Phytophthora*, por lo que es necesario proponer y analizar la eficacia de estrategias alternativas que permitan disminuir los efectos que produce en las plantaciones.

En artículos recientes, hemos demostrado que la configuración de las plantaciones es fundamental en el control de ciertas plagas y fitopatógenos. Por ejemplo, si una variedad de planta es susceptible a un fitopatógen, es recomendable sembrar dejando algunas celdas vacías, que pueden ser ocupadas por una planta más resistente. Sin embargo, en situaciones donde el manejo y cuidados de las plantas sean específicos, la recomendación es considerar plantaciones estructuradas, muy similares a los sistemas milpa. Con el uso de estas estrategias es posible disminuir los efectos de la propagación de fitopatógenos y plagas. Sin embargo, existen condiciones particulares que aún no se han estudiado. Por ejemplo, en el norte del Estado de Puebla, la vainilla se siembra acompañada de una planta tutor, en terrenos con una pendiente considerable. Esta condición marca un cambio sustancial en las condiciones de la propagación de la enfermedad. Por otra parte, existen otra clase de fitopatógenos o plagas que tienen propiedades de movilidad diferentes, por ejemplo la arañita roja realiza caminatas sobre el follaje de las plantas, o la roya del café es propagada a través de las salpicaduras provocadas por las gotas de lluvia. Sin embargo, comparten con *Phytophthora* la característica de propagación sobre las plantas que son adyacentes. Todos estos problemas planteados requieren de atención y pueden ser abordados con las propuestas desarrolladas en nuestro grupo de trabajo.

Trabajos derivados de la investigación sobre aplicaciones de la física en agroecología:

* J. E. Ramírez et al, Phys. Rev. E, 98, 062409 (2018).

* J. E. Ramírez et al, Phys. Rev. E, 101, 032301 (2020).

* D. Rosales Herrera et al, Chaos 31, 063105 (2021).

* D. Rosales Herrera et al, Phys. Rev. E 109, 014304 (2024).

Percolation strategy to improve the production of plants with high pathogen susceptibility

J. E. Ramírez,^{1,2,*} E. Molina-Gayosso,^{3,†} J. Lozada-Lechuga,³ L. M. Flores-Rojas,³ M. I. Martínez,¹ and A. Fernández Téllez¹

¹Facultad de Ciencias Físico Matemáticas, Benemérita Universidad Autónoma de Puebla, Apartado Postal 165, 72000 Puebla, Pue., México

²Departamento de Física de Partículas, Universidad de Santiago de Compostela, E-15782 Santiago de Compostela, España

³Universidad Politécnica de Puebla, Tercer carril del Ejido Serrano, 72640, Juan C. Bonilla, Pue., México



(Received 6 September 2018; revised manuscript received 17 November 2018; published 20 December 2018)

We use percolation theory to propose a strategy that increases the production yield of plants with high susceptibility to a pathogen plague. This strategy consists in sowing a second variety with a lower susceptibility. The percolation threshold is determined as a function of the plant density, the mixture of plants, the pathogen susceptibilities, and the initial percentage of inoculated soil. Moreover, we provide conditions to prevent the formation of a spanning cluster of infected plants. We present an application of this strategy to a particular chili plantation. Under controlled conditions, we measure the pathogen susceptibilities to different strains of *Phytophthora capsici* for three varieties of chili peppers with high commercial value in Mexico. Then we simulate the propagation process of the pathogen on nearest and next-to-nearest-neighbor square lattices. We find that the production yield of plantations with the highest susceptibility can be significantly increased as a result of this novel application of percolation theory.

DOI: [10.1103/PhysRevE.98.062409](https://doi.org/10.1103/PhysRevE.98.062409)

I. INTRODUCTION

Percolation theory is a branch of statistical physics that addresses transport phenomena in porous media [1,2]. It explains, for instance, the conditions under which filtration of water through a wall or how the current flow goes through an electrical mesh can occur [3–6]. The basic idea in percolation theory is to represent porous media as a lattice whose sites either permit the flow (and then are said to be *occupied*) or not. Each site has a probability p (independent of the neighboring sites) of being designated as occupied or, equivalently, a probability $1 - p$ of being designated as *empty* [4]. Evidently the value of p determines if the transport phenomenon takes place or not. If p is too small, then there are too few occupied sites and the transport process cannot occur. Contrarily, if p takes on a value close to 1, then there are plenty of occupied places and one expects transport to occur [4–8]. The case of interest is that in which the number of occupied sites is just enough to allow the transport phenomenon to happen. In such a situation, there is a critical value p_c , called the *percolation threshold*, that bounds from below the values of p for which the transport phenomena will occur. Its determination is one of the fundamental problems in percolation theory [6]. Since finding the percolation threshold analytically is not possible in most applications, computational methods have proved to be an effective alternative [4,6–8].

Percolation theory has been applied in a wide variety of situations, ranging from the study of the formation of galactic structures [9–11] to super-cooled water [12,13],

fragmentation [14–16], porous materials [2,17,18], earthquakes [19–21], forest fires [22–24], deforestation [25], and the properties of the quark-gluon plasma [26–28].

An application of particular interest is the propagation of diseases where a susceptible-infected-recovered (SIR) model is used to determine the critical number of edges that would prevent the propagation of the disease in a certain population [29–37]. In particular, disease propagation models for plants have been proposed in Refs. [38–43] in which different media are considered for pathogen transport, like thin films of water or air.

The interest in applying models like the one described above is due to the great threat that plagues of insects or gastropods, on one hand, and the spread of diseases caused by bacteria, fungi, and oomycetes, on the other, pose on the production of vegetables. The effects range from a reduced production to the complete loss of a plantation or even the transmission of the agent to other plantations sharing the irrigation system, for example. The associated economic losses render the study of the propagation of disease agents and its eventual control necessary.

In the taxonomic class of oomycetes we find the organisms that cause epiphytic interactions with the most destructive effects on crops: the genus *Phytophthora* (from Greek, meaning literally *phyto*, “plant,” and *phthora*, “destroyer” [44]) [45,46]. Long considered as lower fungi, these organisms are more closely related to brown algae and green plants [47,48]. However, they share morphological characteristics with true fungi (Eumycota), such as mycelial growth and the dispersion of spores of mitotic or asexual origin. The latter have a distinctive feature that causes them to have a great impact on the plant kingdom as phytopathogens: their movement by means of flagella [49,50].

These biflagellate zoospores have a mastigoneous flagellum with microfibrils that serve to assist or guide

*Corresponding author for topics related to the model and the simulations. jerc.fis@gmail.com

†Corresponding author for topics related to experimental results. eduardo.molina@up Puebla.edu.mx

movement. They can disperse through water films or soil moisture, including those on the surface of plants. These zoospores emerge from mature sporangia in quantities of 20 to 40 motile zoospores, which swim chemotactically toward the plants [49,51,52].

When the zoospores reach the surface of the roots, they lose their flagella, encyst in the host, and form a germination tube through which they penetrate the surface of the plant [53,54]. However, many species of *Phytophthora* can persist as saprophytes if the environmental conditions are not appropriate but become parasitic in the presence of susceptible hosts [46,52].

Damages produced by the species of the genus *Phytophthora* include rotting in seedlings, tubers, corms, the base of the stem and other organs, staying mainly at the root of many plant species [55]. The variation in infection caused by the different species of *Phytophthora* is associated with the environment conditions, which usually include optimal temperature and humidity, exhibiting a transition of rapid propagation in edaphic media of high humidity. Irrigation is then considered one of the most important means of dissemination since it facilitates the spreading of zoospores [49,56].

Due to the physiology of the oomycetes, most of the fungicides have no effect on them. Therefore, research on non-chemical strategies that minimize or eliminate the propagation of the pathogen is necessary.

In this work we model the propagation of the pathogen *Phytophthora* as a transport phenomenon over a plantation. As happens with some diseases, certain varieties of plants have an intrinsic tolerance to *Phytophthora* [57]. These can inhibit the spread of the pathogen and therefore may be used as protective barriers for plants with less resistance. We incorporate this idea into our model, considering plantations comprising a mixture of varieties with high and low tolerance to the pathogen. Since it is *a priori* unknown whether one particular seed of a given variety will yield a nontolerant plant, we assume the latter are uniformly distributed over the plantation.

We use percolation theory to propose a strategy that suppresses or at least minimizes the spread of *Phytophthora capsici* in chili plantations. We are interested in predicting the conditions on the parameters of the crops that reduce the propagation of the disease and maximize the total plant production. To this end, we model plantations as square matrices with a plant in each of their cells.

We report the pathogen susceptibility for three varieties of chili plants. With these data we are able to find a way to prevent the disease from propagating over the whole plantation for the most susceptible chili variety. By mixing with a second chili variety, our model yields the mixing proportion and the plant density for a given initial percentage of inoculated soil that would contain and prevent the pathogen from spreading.

This paper is organized as follows. In Sec. II, we describe the model for pathogen propagation over a plantation in terms of percolation theory. Then we find the percolation threshold for these systems implemented in regular lattices as a function of the mixing proportion, the pathogen susceptibilities, and the initial percentage of inoculated soil. Section III describes the experimental setup for the determination of the pathogen susceptibility of four varieties of *Phytophthora* for three commercially relevant varieties of chili: “Arbol,” “Serrano,”

TABLE I. Percolation threshold for different regular lattices. Data taken from Ref. [4].

Lattice	p_c
2N square	0.592...
3N square	0.407...
Triangular	0.5
Hexagonal	0.697...

and “Poblano.” In Sec. IV we report the susceptibility measurements and obtain the mixing thresholds for which the disease will only propagate over finite clusters even if all cells in the plantation are sowed. In addition, for the case of high susceptibility measured for the “Arbol” variety when exposed to *P. capsici*, we determine by computer simulation the total production yield as a function of the occupation probability and the mixing proportion with a second chili variety of lower susceptibility. A discussion and a comparison with the alternate rows sowing strategy is included in Sec. V. Section VI contains the conclusions of this work.

II. MODEL

The basic percolation model studies the formation of clusters on regular lattices with N sites, where each site is available to the process with a probability p . It is of particular interest to determine the percolation threshold p_c , that is, the minimum probability at which a spanning cluster extending across the percolating system appears. This critical density depends on the properties of the lattice, as illustrated in Table I. There we show the percolation threshold for the nearest (denoted by 2N) and next-to-nearest-neighbor (denoted by 3N) square, triangular, and hexagonal lattices.

A. Percolation threshold

In this work the sites in the lattice represent plants of two different varieties growing on specific soil. Each variety has a particular pathogen susceptibility, which is the probability of being infected by a specific pathogen. We denote by A and B the different plant varieties in the plantation, while χ_A and χ_B denote their pathogen susceptibilities.

We consider a regular lattice with a probability of occupation p . The available sites in the lattice can be occupied by two different types of plants, distributed in a homogeneous way according to a certain proportion. We define M as the probability that an available site is occupied by a plant of variety A , so $(1 - M)$ it is the probability that an available site is occupied by a plant of variety B . We are interested in studying the spread of the disease on plants which can get infected. Because the pathogen susceptibilities may be different from one, then the spread of the disease occurs on a percolating system with an effective probability p_{eff} that depends explicitly on p , χ_A , χ_B , and M .

In a percolating system with given p , χ_A , χ_B , and M , the average number of effective sites available for the spread of the disease can be written as $N_{\text{dis}} = \langle N_A \rangle + \langle N_B \rangle$, where

$\langle N_{A,B} \rangle$ is the average number of susceptible sites of type A or B , which can be calculated as

$$\langle N_A \rangle = NM\chi_A p; \tag{1}$$

$$\langle N_B \rangle = N(1 - M)\chi_B p. \tag{2}$$

In addition to the average number of plants that can get infected, it is necessary to take into account the fraction of cells that are inoculated with the pathogen. These can be located in occupied sites or in plants that are resistant. Even in these cases, the pathogen may spread to neighboring plants. Defining I as the probability that a cell in the lattice is inoculated, we have that the average number \mathcal{N} of cells through which the propagation process can occur is

$$\mathcal{N} = Np_{\text{eff}} = N_{\text{dis}} + (N - N_{\text{dis}})I, \tag{3}$$

where the second term on the right-hand side has been added to consider the inoculated sites that match the situation described above. This last equation corresponds to a percolation process that occurs on a lattice with an effective probability given by

$$p_{\text{eff}} = I + (1 - I)[M\chi_A + (1 - M)\chi_B]p. \tag{4}$$

Equation (4) is crucial, since it determines the formation properties of clusters of plants that have been infected by the pathogen, including those plants that do not manifest the disease but can propagate it. The existence of the spanning cluster of infected plants occurs when the value of p_{eff} in Eq. (4) coincides with that of the percolation threshold of the lattice. In that case, the percolation threshold of the system is given by

$$p_c^* = \frac{p_c - I}{(1 - I)[M\chi_A + (1 - M)\chi_B]}. \tag{5}$$

In general, there is not a direct way to compare p_c^* to p_c . However, it is possible to determine specific conditions for which a spanning cluster will not exist. If we consider that p_c^* can only take values between zero and one, then the no percolation condition for the values of I , M , χ_A , and χ_B is $(1 - I)[M\chi_A + (1 - M)\chi_B] \leq p_c - I$. This is an important condition because once knowing the pathogen susceptibilities of the plants, we can determine the proportion M that guarantees that no percolating cluster is formed, despite a fraction I of soil area might be inoculated.

B. Disease incidence

Another important parameter that can be calculated is the extent of disease incidence on the sown plants. Note that independently of the lattice, the pathogen can spread on plants that are susceptible and belong to the same cluster.

Because some pathogens can present latency stages when they are in an adverse environment, any point in the lattice can be the source of infection, even a place with no plant or with a plant resistant to the pathogen. This fact highly complicates the determination of an analytical result for the percentage of the plantation that can be damaged by the spread of the disease. If the initial point of infection is an empty place or a place occupied by a plant resistant to the pathogen, then the disease can be transmitted to more than

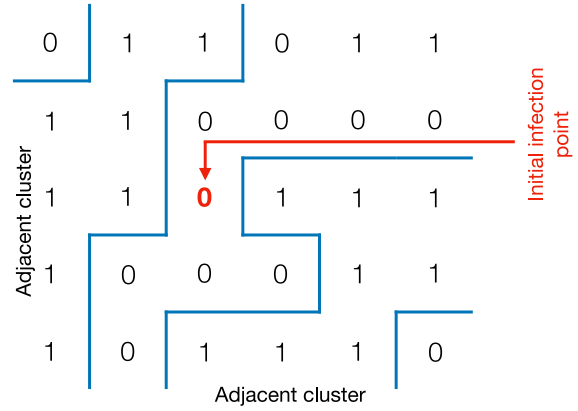


FIG. 1. Example of an initially infected point (red zero) surrounded by two adjacent and disjoint clusters delimited by a blue line for a nearest-neighbor square lattice with $p = 0.6$.

one adjacent cluster as shown in Fig. 1, where an initial point of infection allows the pathogen to spread over two disjoint clusters. For this reason we expect the average number of cells where the pathogen causes damage to be slightly larger than the average cluster size, for $p_{\text{eff}} \sim p_c$, as a result of the connecting effect between disjoint clusters by the initial infection point. On the other hand, for $p_{\text{eff}} < p_c$, we expected that the contribution of the initial point of infection be through finite clusters or isolated sites. Finally, for $p_{\text{eff}} > p_c$, the initial point of infection belongs to the spanning cluster as p_{eff} takes values greater than the percolation threshold. Consequently, if there is more than one initial point of infection in the system, we expect the appearance of cells connecting two adjacent disjoint clusters to magnify. Evidently, this effect does not scale linearly, since it may happen that two initial points transmit the disease to the same cluster. In Sec. IV we will discuss the implications of considering several initial points.

Finally, if we know the pathogen susceptibilities χ_A and χ_B of two varieties, then we can predict the mixture of seeds and the fraction of sown cells that will maximize the total yield obtained from the whole production of A and B , which may be computed as the number of cells for which the pathogen could not spread.

C. Simulation on square lattices

Traditionally, crops are planted in parallel rows on the soil, so that the seeds are sown in a square lattice-type arrangement. The best approximation to represent the system is a Boolean matrix whose values on each entry depend on whether seed is deposited or not in the cell. The cells are spaced according to the maximum displacement length that the pathogen can travel. We do not know *a priori* what value corresponds to a given cell (this is, we do not know whether a seed was sown there). Therefore, we assign a 1 to each entry in the matrix according to the occupation probability p . Given a proportion mixture $0 < M < 1$, we assign randomly to each occupied cell (i.e., to each entry in the matrix with a value of 1) a plant variety A or B . Specifically, we generate for each cell a random number x between zero and one and define that, if $x < M$, then a plant of variety A has been sown. Otherwise, it

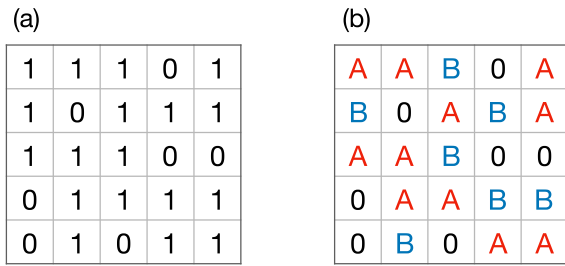


FIG. 2. (a) Representation of a percolating system with occupation probability p as a square matrix. (b) Representation of plants of types A and B randomly sown in the cells of the matrix according to a predefined proportion $M = 0.6$.

means that a plant of variety B has been sown. Figure 2 shows an example of the random configuration of the mixture of the two plant varieties represented as a percolating system.

The inoculated cells in this initial configuration are taken in a uniform random way over the matrix with a probability I , which represents the ratio of inoculated cells in the matrix.

Once the cells are inoculated, the pathogen might or might not be propagated to neighboring plants, depending on the pathogen susceptibility χ of each variety of plant. In practice, a plant of type A (B) gets infected and develops the disease if a generated random number is less than χ_A (χ_B); otherwise, the plant remains healthy. If the plant is infected and becomes sick, then its cell value is changed from one to zero. Figure 3 shows an outline of this infection propagation process. The matrix in the upper left corner represents the initial distribution of plants sown with a mixture M , while the matrix on the right shows the result of exposure to the pathogen.

Finally, we take as the production yield for each plant variety the number of plants still alive after the infection has spread. With this method, we simulate the behavior of the plant production yield as a function of the probability p and the mixture M .

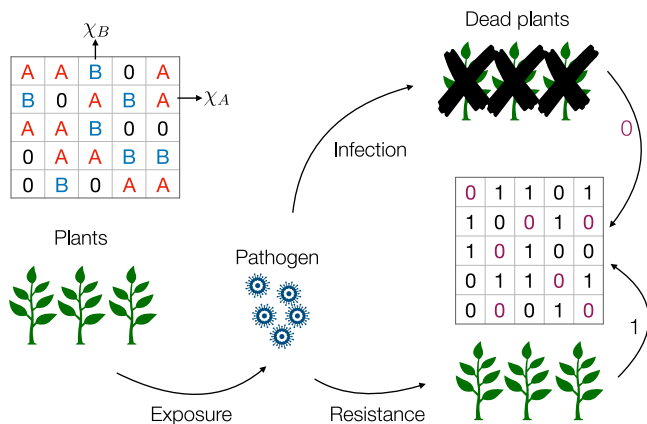


FIG. 3. The pathogen propagation process. The initial configuration (top left) is exposed to the pathogen and each plant has a probability I of being infected. The infected plants are considered as dead and the respective cells in the matrix are marked with a purple zero (right).

III. MATERIAL AND METHODS

A. Substrate preparation

The substrate preparation was carried by mixing peat moss and sieved soil (2-mm mesh) in a 1:2 volume-volume mixture. The homogeneous mixture was placed in plastic double bags of 6 kg of high density polyethylene. The bags with the substrate were sterilized in an electric autoclave at 121 °C and 6.8 kg/cm² for 30 min for 2 consecutive days.

B. Preparation and treatment of seeds

Three varieties of chili seed were used: “chile de Arbol” from Michoacán, “chile Serrano” from the state of Nayarit, and “chile Poblano” from the state of Puebla. For each one, 100 seeds without deformities were selected. Groups of 100 seeds were selected and weighted for carrying the tests. Each pack of seeds was deflated by adding approximately 20 ml of hydrogen peroxide (9 vol. H₂O₂) in a beaker for a period of 20 min and then rinsed with distilled water for three times and allowed to stand for 2 days immersed in sterile distilled water to promote germination.

C. Preparation of bioassays

For each bioassay, aluminium trays of approximately 3 kg capacity were used. To each tray was added 1.5 kg of sterile substrate, and on it the seed was spread homogeneously and finally covered with 1 kg more of substrate, moistened with enough water, and covered with black bags.

The trays were watered daily with enough water to maintain the humidity until beginning to see the buds of seedlings. The initial growth was observed eight days after sowing. From this moment, it was fertilized every 7 days with 1.9 g/l of the fertilizer blue Nitrofoska.

D. Inoculation of soil with oomycetes

The microorganisms used were taken from the phytopathogenic oomycete strain collection of the Biotechnology Academic Program at the Universidad Politécnica de Puebla. The isolates were reactivated in a selective agar-corn medium added with a mixing of antibiotics (pimaricin, 0.01 g/l; ampicillin, 0.250 g/l; rifampicin, 0.01 g/l).

Each oomycete used was inoculated in the same sterile substrate used for the preparation of the trays. Segments of the growths were inoculated in plastic bags containing 500 g of substrate. The bags were mixed by shaking every 2 days for 3 weeks to ensure the growth of the oomycete throughout the substrate. They were incubated at room temperature. For each inoculated substrate the presence of the respective oomycete was verified by seeding 1 ml of a 1:9 dilution inoculated substrate: water in cornmeal medium-agar added with antibiotics (pimaricin, 0.01 g/l; ampicillin, 0.250 g/l; rifampicin, 0.01 g/l). It was incubated at 27 °C for 5 days.

E. Inoculation of trays

On average, each tray planted contained about 80 seedlings and each of the oomycetes was inoculated into three trays corresponding to the three varieties of chili. The inoculation

TABLE II. Experimental results of the pathogen susceptibilities for different *Capsicum* varieties: “Chile Serrano” (χ_S), “Chile de Arbol” (χ_A), and “Chile Poblano” (χ_P), exposed to several *Phytophthora* isolates.

Oomycete	χ_S	χ_A	χ_P	Kruskal-Wallis test
PcV01	0.60	1.0	0.89	Pr < 0.0001 A = P
PcV51	0.46	0.27	0.76	Pr < 0.0006
PcV77	0.64	0.36	0.04	Pr < 0.0001 but A = P
PcV90	0.40	0.10	0.19	Pr < 0.0002 all the same
Blank test	0	0	0	

was carried out by adding in the center of each tray 10 g of soil infested by the oomycete corresponding to the treatment. Then it was irrigated with water to favor infestation. Before the inoculation, a census of plants was carried out for each tray.

The fertilization of the plants was stopped at the microorganism inoculation. However, the humidity was maintained at field capacity during the whole time of the test, and 35 days after sowing, live plants were counted in each tray and the survival percentage was calculated.

IV. RESULTS

In this section we show results for the pathogen susceptibility of chili plants of the “Arbol,” “Serrano,” and “Poblano” varieties exposed to the pathogen oomycete *P. capsici*. We also present the conditions predicted by our model that maximize the production of mixtures of two of these varieties of chili plants when the portion of inoculated cells is 1%, 5%, and 10%.

A. Susceptibility of chili varieties exposed to different *P. capsici* isolates

We obtained the survival rate experimentally by exposing a number of plants to the pathogen and noting the number of alive plants after the period of time mentioned in Sec. III. We denote the survival rate of a plant type exposed to a pathogen (expressed as a percentage) as \mathcal{P} , then, the pathogen susceptibility is calculated as

$$\chi = 1 - \frac{\mathcal{P}}{100}. \quad (6)$$

Table II shows the pathogen susceptibility calculated with Eq. (6) for the varieties of “Serrano” (S), “Arbol” (A), and “Poblano” (P) plants of chili exposed to various strains of the pathogen *P. capsici* denoted by PcV and a number to distinguish them from each other.

We actually measured susceptibilities for 20 different strains (including their respective blank tests). These measurements were carried out in a period of approximately 5 months since the procedure described in Sec. III was repeated for all 20 strains in a small green house. The space and time limitation precluded the measurements to be performed more than once. We report susceptibility values for the four strains we consider to be representative for the analysis done in this study. On the other hand, we used Kruskal-Wallis tests to

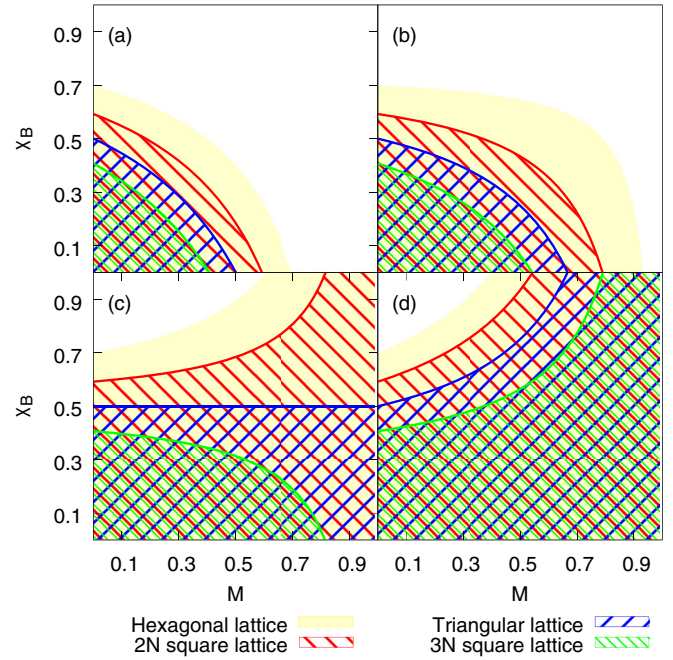


FIG. 4. Examples of conditions for no percolation in regular lattices when the density of inoculated cells is small ($I \rightarrow 0$) for values of $\chi_A = 1.00$ (a), 0.75 (b), 0.50 (c), 0.25 (d), when the pathogen propagates over 2N square (red inverse diagonal filled), 3N square (green inverse diagonal filled), triangular (blue diagonal filled), and hexagonal (yellow filled) lattices.

determine that at least two of the compared groups per strain are significantly different whenever the distribution of their data was not a normal distribution. In Table II Pr denotes the probability that a false negative occurred. The small values we obtained mean the three chilis actually have different susceptibilities to the pathogen.

Using the data in Table II, we found the conditions on M and p that optimize the production of the three possible mixtures of two varieties of chili: $A-P$, $A-S$, and $P-S$.

B. Regular lattices

As mentioned in Sec. II A, depending on the values of the pathogen susceptibility of each plant, we can determine the values of M for which the pathogen will only spread on finite clusters, even if all cells are sown. In Fig. 4 we show the combinations of pathogen susceptibility χ_B and mixture M that prevent the formation of the spanning cluster for fixed $\chi_A = 1.00, 0.75, 0.50,$ and 0.25 in different regular lattices in the limit $I \rightarrow 0$, corresponding to a single initial inoculation point.

In an analog way, we determined the conditions on M for given values of I that produce no percolation for the pathogen susceptibilities found experimentally. This allowed us to compute the critical mixture M at which we predict the infection will only spread to finite clusters even if all cells are sown, as is shown in Fig. 5. In this context, $M = 0$ ($M = 1$) means only plants with the highest (lowest) susceptibility were sown. Note that the case $M = 1$ can occur as long as one of the plants has a susceptibility small enough to

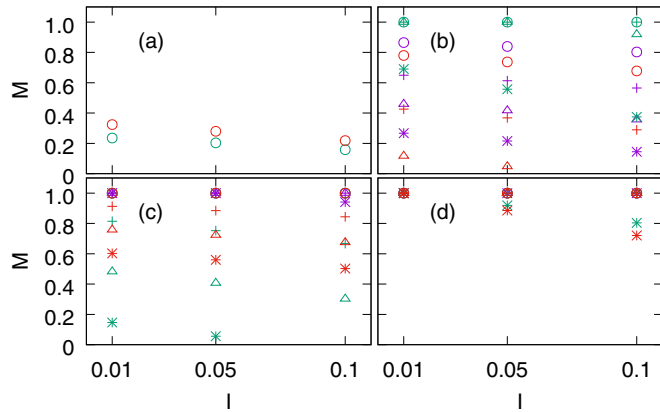


FIG. 5. Conditions for no percolation in 2N (crosses), 3N (stars), triangular (triangles), and hexagonal (circles) lattices of different chili plants mixtures: *A-P* (purple), *A-S* (green), and *P-S* (red) exposed to the strains PcV01 (a), PcV51 (b), PcV77 (c), and PcV90 (d) considering three values of inoculated cells density $I = 0.01, 0.05, \text{ and } 0.10$.

suppress the pathogen spreading. Such is the case for the PcV90 strain for which the three varieties of chili have small susceptibilities as shown in Fig. 5(d). As it can be seen in Fig. 5, almost all combinations of chili plants in almost all the regular lattices yield $M = 1$. On the other hand, for the cases of strains PcV51, Fig. 5(b), and PcV77, Fig. 5(c), there are several values of the mixture different from 1. In these cases, a more resistant variety of chili must be introduced to avoid the spread of the disease over the most susceptible plant. The most interesting case occurs when plants are exposed to the strain PcV01, Fig. 5(a), since we only found mixing values where the disease does not spread for hexagonal lattices. This singular case is analyzed in Sec. IV C, where we determine conditions for which the production of plants is optimized.

C. Simulation on square lattices

To estimate the production yield as a function of the probability of occupation p and the mixture M , we perform simulations in square matrices of size 100×100 . We start with initial values of 0.05 for both p and M . First, we increase

the value of p up to 0.95, in increments of $\Delta p = 0.05$. We then increase the value of M in steps of size $\Delta M = 0.05$ repeating the scan in p for each value of M , up to $M = 0.95$. The simulation was performed 2×10^4 times for each pair of values of p and M , for the three possible chili combinations: *P-S*, *A-P*, and *S-A*, using the pathogen susceptibilities reported in Table II.

In Fig. 6 we show the production yield obtained by computer simulation for the *P-S* mixture in the presence of the pathogen PcV01 with different densities of inoculated soil ($I = 0.01, I = 0.05, \text{ and } I = 0.1$) in a nearest-neighbor square lattice. The darkest areas indicate the values of density of plants p and mixture M for which the production yield is maximized.

Figure 7 shows level curves of the production yield for different densities of inoculated cells in nearest neighbors (red lines) and next-to-nearest-neighbor (blue lines) square lattices. The production levels were obtained through extrapolation using cubic splines between adjacent points in the p - M plane. Then the level curves of the results obtained by computer simulation were determined. The curves on the graphs in Fig. 7 bound the region where the maximum production yield reaches a certain value, which is indicated by a label on each line.

Finite-size effects on the production yield curves

As is usual in percolation theory some dependence of the observed quantities on the system size is expected: the so-called *finite-size effects* [58–61]. In our case the system size corresponds simply to the matrix size ($L \times L$) which we use in our simulations. To observe these effects we study the behavior of the 35%, 45%, and 55% production level curves for the *P-S* mixture shown in Fig. 7(a) as a function of L . Figure 8 shows these curves for $I = 0.01$ in a nearest-neighbor square lattice for different matrix sizes.

It is clear that dependence of the production curves on L is rapidly lost. For occupation probabilities below 0.6 the curves are practically independent of L , in agreement with the fact that the effective probability of the simulated systems is low ($p_{\text{eff}} \leq 0.52$ for all M) and therefore the process propagates over finite clusters. In contrast, for larger p values, larger

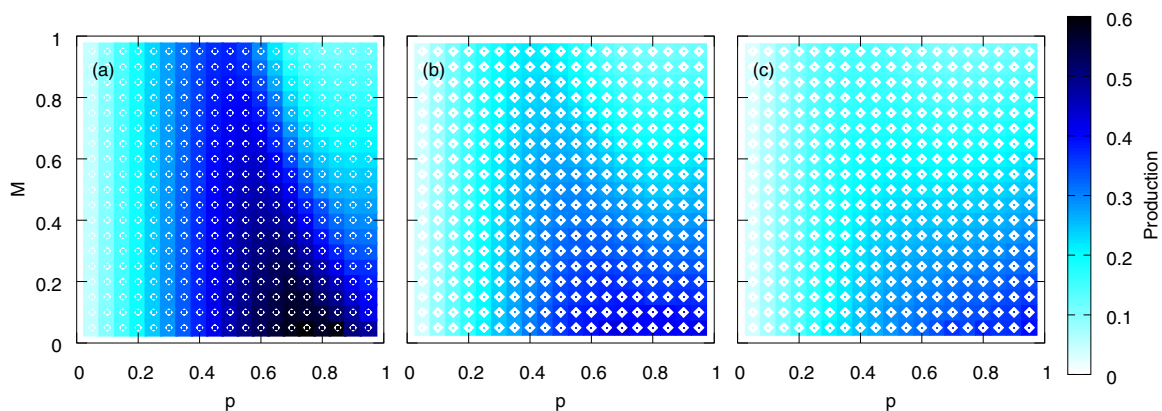


FIG. 6. Simulation results for the production of cells with alive plants after the spreading of the disease on the chili mix *P-S* for values of inoculated cells $I = 0.01$ (a), 0.05 (b), and 0.10 (c). Regions in dark represent the higher production yields.

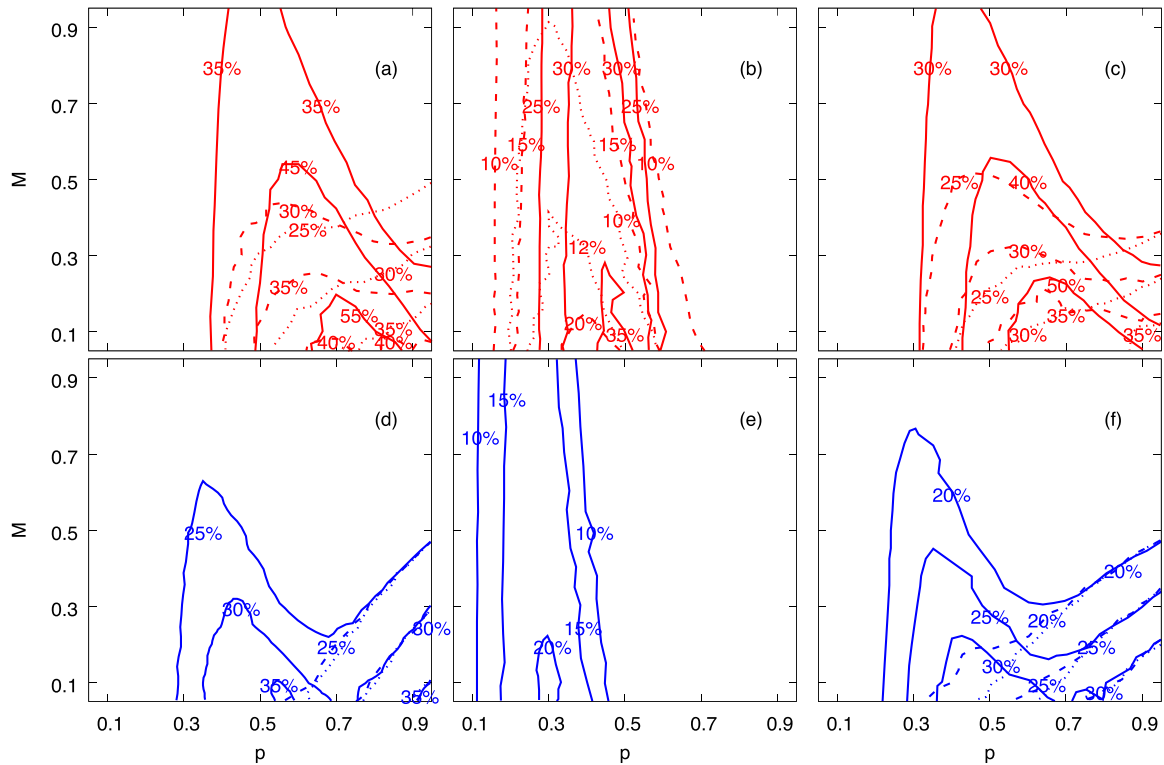


FIG. 7. Level curves for the production yield in terms of the density of plants and the mixture for the three combinations of chili plants at different inoculation densities $I = 0.01$ (solid lines), $I = 0.05$ (dashed lines), and $I = 0.10$ (dotted lines). Top row (red curves) correspond to a nearest-neighbor square lattice for the P - S (a), A - P (b), and S - A (c) mixtures. Bottom row (blue curves) correspond to a next-to-nearest-neighbor square lattice for the P - S (d), A - P (e), and S - A (f) mixtures.

clusters are formed with corresponding larger fluctuations of their probability distribution. Furthermore, the absolute num-

ber of initially inoculated sites grows as IL^2 so the number of inoculated sites is, for example, two orders of magnitude less in a system with $L = 20$ than that of a system with $L = 200$. This means that the number of explored clusters for the propagation of the infection is much limited in small size systems.

V. DISCUSSION

In this paper we proposed a strategy based on percolation theory on regular (triangular, square, and hexagonal) lattices to optimize the production of crops in a plantation. The strategy consists in sowing two varieties of plants with different susceptibilities to a specific pathogen arranged as a percolating system in order to maximize the number of plants that survive an infestation. We assumed that the lattice spacing in the percolation system coincides with the maximum distance that the pathogen can travel before entering a state of dormancy or before dying due to starvation.

We were able to establish a relationship between the percolation threshold of systems with two different probabilities for the occurrence of the propagation process and the parameters of the plantation. Namely the pathogen susceptibilities χ_A and χ_B of each type of plant, the mixture M , the fraction of sites that can initiate infection I , and the percolation threshold of the lattice in which the plants are sown. We also found that, under particular conditions of pathogen susceptibility, there are values of the mixture M for which the disease will only propagate on finite clusters even if all the soil is sown.

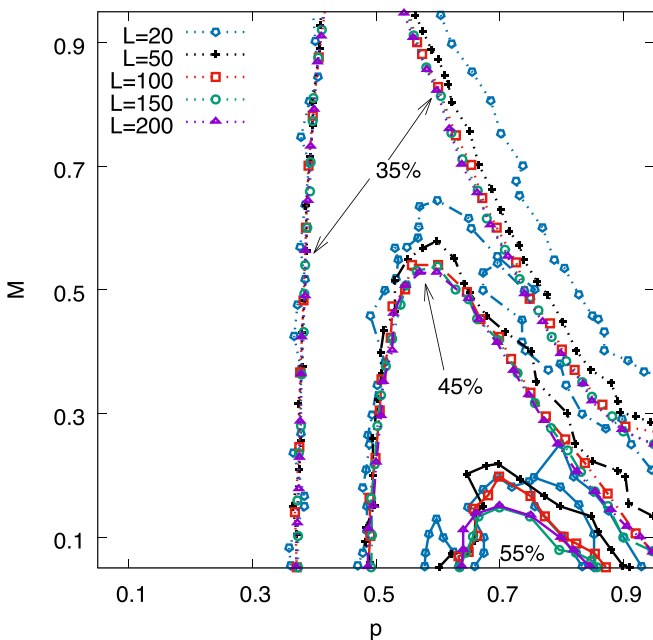


FIG. 8. Finite-size effect on the production yield lines for the P - S mixing exposed to PcV01 with a percentage of inoculated soil $I = 0.01$ in a nearest-neighbors square lattice.

We experimentally measured the pathogen susceptibility to different varieties of the *Phytophthora* pathogen of three chili varieties: “Serrano,” “Arbol,” and “Poblano” which are of commercial value in Mexico. We found that for the pathogens catalogued as PcV51, PcV77, and PcV90, there are values of the mixture M for which the infection will only spread on finite clusters, independently of the regular lattice that is considered. On the other hand, we found that the mortality rate of the plants in presence of PcV01 is relatively high, so it is not possible to find mixing values for which the infection propagates on finite clusters. For this particular case, we determined by computer simulation the production yield of the three possible pairs of plants for three different percentages of inoculated soil $I = 0.01, 0.05,$ and 0.10 . We found the production yield is highly sensitive to the amount of soil inoculated and there is a considerable difference in production yield for the extreme values of I . In addition, the production yield for the next-to-nearest-neighbor lattice is lower than that for the nearest-neighbor lattice due to the fact that in the 3N square lattice, the number of coordination is larger than in the 2N square lattice, which means that the pathogen has more options to spread.

In the most drastic case of pathogen susceptibility, the “Arbol” variety was measured to have $\chi_A = 1$, which means the infection will spread over all the plants regardless of the percentage of inoculated land when all the soil is sown. However, when mixed with the “Serrano” variety ($\chi_S = 0.6$) on a nearest-neighbor square lattice, we found total production level curves of 50%, 35%, and 30% of the total cells for inoculated soil levels of $I = 0.01, 0.05,$ and 0.10 , respectively. On the other hand, on a next-to-nearest-neighbor square lattice we found production level curves around 30% regardless of the fraction of the soil inoculated. These results show that the production of “Arbol” could be improved if sown in combination with a second variety of chili plant.

We compared the predictions of our model to the simulated production yield for a crop with a mixing of two chilis sowed in alternate rows of the lattice. That is sowing one of the varieties in all sites of a row and filling the next row with the other type of chili. We found the production yield for each of the three combinations of chilis does not depend on the coordination number of the lattice nor on the fraction of soil initially inoculated. For these varieties with pathogen susceptibilities close to 1 the production yield is given by $1 - (\chi_A + \chi_B)/2$. For example, in the S - A mixing exposed to PcV01, on the average, half of the initially inoculated plants will be of the variety A and then the corresponding rows will be completely lost since $\chi_A = 1$. Consequently, the rows with variety S will in fact be exposed to the pathogen and only the resistant plants will survive. At the same time, the infected plants of variety S will continue propagating the pathogen to the next row and so on. At the end of the propagation process, only resistant plants of the variety S will be alive, which corresponds to 20% of all cells (since the mixing proportion is 50% and $\chi_S = 0.6$). And the pathogen will spread over all the lattice. On the other hand, using our model, there is a production yield curve corresponding to 50% ($\sim 10\%$ of variety $A + \sim 40\%$ of variety S).

In Fig. 9 we show the yield production for the alternate rows strategy and the maximum percentage observed for the

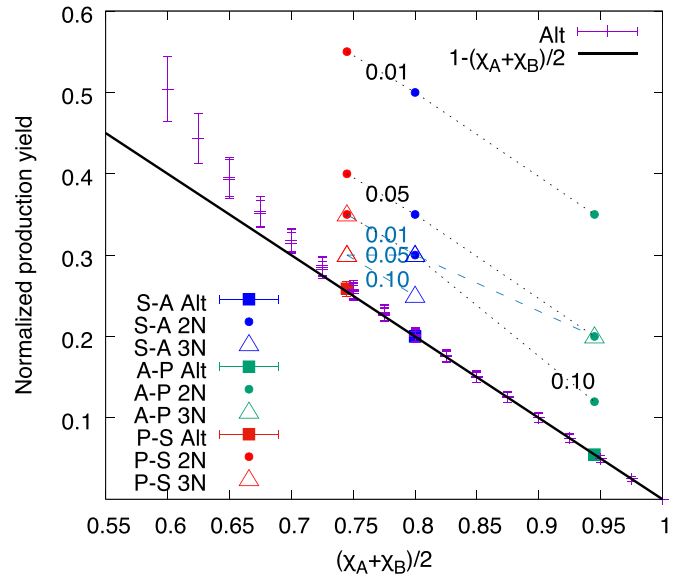


FIG. 9. Comparison of the production yield between the alternate rows sowing (filled squares) and the percolation strategy for the P - S (red), A - P (green), and S - A (blue) mixings, for plants exposed to PcV01. Simulations of the percolation strategy in 2N (filled circles) and 3N (triangles) lattices for different fractions of inoculated soil ($I = 0.01, 0.05, 0.1$) are shown. Production yield of systems sowed in alternate rows with different combinations of pathogen susceptibilities (purple points) agree with $1 - (\chi_A + \chi_B)/2$ (black curve) for high susceptibilities values.

percolation strategy in 2N and 3N square lattices. Simulations of alternate rows sowing for other combinations of pathogen susceptibilities were performed (see the purple points in Fig. 9). Note that for those systems where the pathogen susceptibility is high for both plant varieties, the normalized production yield is well fitted by $1 - (\chi_A + \chi_B)/2$. Finally, the percolation strategy presented here predicts a better production yield than the alternate rows sowing strategy, even in those systems where the pathogen can reach next to nearest neighbors in the square lattice for the three analyzed fractions of inoculated soil.

VI. CONCLUSIONS AND PERSPECTIVES

In this work, we have presented and implemented a model based on percolation theory to avoid the spreading process of a pathogen with the capability of movement (by flagella) through plants with high susceptibility by the sowing of a plant mixture with less pathogen susceptibility. We have determined the percolation threshold and the no percolation condition for these systems considering the following variables: density of cells sown, pathogen susceptibilities, the portion of plant mix, and the percentage of inoculated soil. This strategy can be applied in a whole variety of cases. Also, for those systems where it is not possible to determine the no percolation conditions, we presented the corresponding Monte Carlo simulation. The main result of this approach is the possibility to raise the production yield of the plant with high pathogen susceptibility, even when the yield production is close to zero under traditional sowing conditions.

The strategy presented here could help farmers to select the type of plants that would give the best production yield on their land without applying any pesticides or chemical products. The required parameters to predict the production yield for a given mixture of plants are just the percentage of soil initially inoculated and the pathogen susceptibilities of the plants involved. One has to consider that applying this model to a real-life situation, farmers should now be interested in the physical and chemical properties of harmful microorganisms that inhabit their land and in the response of the desired plants to sow in the presence of those pathogens. These properties would enable them to determine the sowing conditions that would optimize the harvest.

Since the model allows for available cells, a third plant variety can be added in the empty spaces. This would clearly permit farmers to better exploit their agronomic resources with the only restriction of choosing a more resistant variety of plant. This proposal is in agreement with polyculture, which is promoted as a way for sustainable use of soils.

The model could be straightforwardly extended to assess the effect of additional variables of the pathogen dynamics on

the propagation of the disease, giving a more accurate prediction of the production yield. For example, reinfection and recovery of some plants were observed on our experiments. The plant reinfection lapse and the recovery time could be measured and implemented in our model using an SIR model approach.

Finally, some other types of variables might also be included, such as the care provided by the farmer or the possibility of having more than one type of pathogen in the field. This occurs, for example, with *P. capsici*, whose subvarieties can all be found in the same parcel.






ACKNOWLEDGMENTS

J.E.R. acknowledges financial support from VIEP-BUAP (Grant No. VIEP2017-123). E.M.-G. acknowledges financial support from SAGARPA (Contract No. DF1600000998 SNITT/245). The computer simulations were performed at the LNS-BUAP. We also thank M. A. García-Ariza for his valuable comments and help to improve this manuscript.

-
- [1] S. R. Broadbent and J. M. Hammersley, *Math. Proc. Cambridge Philos. Soc.* **53**, 629 (1957).
- [2] M. Sahini and M. Sahimi, *Applications of Percolation Theory* (CRC Press, London, 2014).
- [3] S. Kirkpatrick, *Rev. Mod. Phys.* **45**, 574 (1973).
- [4] D. Stauffer and A. Aharony, *Introduction To Percolation Theory*, revised 2nd ed. (CRC Press, Boca Raton, FL, 2014).
- [5] G. Grimmett, *Percolation*, Grundlehren der mathematischen Wissenschaften (Springer, Berlin, 2013).
- [6] A. A. Saberi, *Phys. Rep.* **578**, 1 (2015).
- [7] D. Stauffer, *Phys. Rep.* **54**, 1 (1979).
- [8] D. Stauffer, A. Coniglio, and M. Adam, in *Polymer Networks*, edited by K. Dušek (Springer, Berlin, 1982), pp. 103–158.
- [9] P. E. Seiden and L. S. Schulman, *Adv. Phys.* **39**, 1 (1990).
- [10] A. Klypin and S. F. Shandarin, *Astrophys. J.* **413**, 48 (1993).
- [11] L. S. Schulman and P. E. Seiden, *Science* **233**, 425 (1986).
- [12] H. E. Stanley, *J. Phys. A: Math. Gen.* **12**, L329 (1979).
- [13] C. K. Hu, *J. Phys. A: Math. Gen.* **16**, L321 (1983).
- [14] G. Wagner, A. Birovljev, P. Meakin, J. Feder, and T. Jøssang, *Phys. Rev. E* **55**, 7015 (1997).
- [15] I. Kantorovich and E. Bar-Ziv, *Combust. Flame* **113**, 532 (1998).
- [16] X. Campi, H. Krivine, N. Sator, and E. Plagnol, *Eur. Phys. J. D* **11**, 233 (2000).
- [17] M. Sahimi and D. Stauffer, *Chem. Eng. Sci.* **46**, 2225 (1991).
- [18] B. Ghanbarian, H. Daigle, A. G. Hunt, R. P. Ewing, and M. Sahimi, *J. Geophys. Res.: Solid Earth* **120**, 182 (2014).
- [19] M. Sahimi, *Physica A* **186**, 160 (1992).
- [20] B. K. Chakrabarti, *Rep. Adv. Phys. Sci.* **01**, 1750013 (2017).
- [21] A. Sakhaee-Pour and A. Agrawal, *J. Pet. Sci. Eng.* **160**, 152 (2018).
- [22] T. Ohtsuki and T. Keyes, *J. Phys. A: Math. Gen.* **19**, L281 (1986).
- [23] T. Beer and I. Enting, *Math. Comput. Model.* **13**, 77 (1990).
- [24] B. Drossel and F. Schwabl, *Phys. Rev. Lett.* **69**, 1629 (1992).
- [25] F. Taubert, R. Fischer, J. Groeneveld, S. Lehmann, M. S. Müller, E. Rödig, T. Wiegand, and A. Huth, *Nature* **554**, 519 (2018).
- [26] G. Baym, *Physica A* **96**, 131 (1979).
- [27] X. Campi, *J. Phys. A: Math. Gen.* **19**, L917 (1986).
- [28] J. E. Ramírez, A. Fernández Téllez, and I. Bautista, *Physica A* **488**, 8 (2017).
- [29] D. S. Callaway, M. E. J. Newman, S. H. Strogatz, and D. J. Watts, *Phys. Rev. Lett.* **85**, 5468 (2000).
- [30] M. E. J. Newman and D. J. Watts, *Phys. Rev. E* **60**, 7332 (1999).
- [31] C. Moore and M. E. J. Newman, *Phys. Rev. E* **61**, 5678 (2000).
- [32] M. E. J. Newman, *Phys. Rev. E* **66**, 016128 (2002).
- [33] M. E. J. Newman, *Phys. Rev. Lett.* **89**, 208701 (2002).
- [34] L. Meyers, *Bull. Am. Math. Soc.* **44**, 63 (2007).
- [35] E. B. Postnikov and I. M. Sokolov, *Math. Biosci.* **208**, 205 (2007).
- [36] J. C. Miller, *Phys. Rev. E* **80**, 020901 (2009).
- [37] E. Massaro and F. Bagnoli, *Phys. Rev. E* **90**, 052817 (2014).
- [38] B. Dybiec, A. Kleczkowski, and C. A. Gilligan, *Phys. Rev. E* **70**, 066145 (2004).
- [39] M. W. Shaw, *Annu. Rev. Phytopathol.* **32**, 523 (1994).
- [40] D. J. Bailey, W. Otten, and C. A. Gilligan, *New Phytol.* **146**, 535 (2000).
- [41] G. J. Gibson, W. Otten, J. A. N. Filipe, A. Cook, G. Marion, and C. A. Gilligan, *Stat. Comput.* **16**, 391 (2006).
- [42] W. Otten and C. A. Gilligan, *Eur. J. Soil Sci.* **57**, 26 (2006).
- [43] C. C. Mundt and K. E. Sackett, *Ecosphere* **3**, art24 (2012).
- [44] T. Reglinski, M. Spiers, J. Taylor, and M. Dick, *New Zealand J. Forestry* **54**, 16 (2010).
- [45] M. Thines and S. Kamoun, *Curr. Opin. Plant Biol.* **13**, 427 (2010).
- [46] K. H. Lamour, R. Stam, J. Jupe, and E. Huitema, *Mol. Plant Pathol.* **13**, 329 (2011).
- [47] P. van West, A. A. Appiah, and N. A. Gow, *Physiol. Mol. Plant Pathol.* **62**, 99 (2003), root Diseases.

- [48] M. W. Dick, in *Systematics and Evolution*, edited by D. J. McLaughlin, E. G. McLaughlin, and P. A. Lemke (Springer, Berlin, 2001), pp. 39–72.
- [49] D. C. Erwin and O. K. Ribeiro, *Phytophthora Diseases Worldwide* (American Phytopathological Society Press, Minnesota, 1996).
- [50] See Supplemental Material at <http://link.aps.org/supplemental/10.1103/PhysRevE.98.062409> for a microscope video showing the slight movements of *Phytophthora*.
- [51] E. A. Bernhardt and R. G. Grogan, *Phytopathology (USA)* **72**, 507 (1982).
- [52] A. R. Hardham, *Mol. Plant Pathol.* **6**, 589 (2005).
- [53] B. Feng, P. Li, H. Wang, and X. Zhang, *Microb. Pathog.* **49**, 23 (2010).
- [54] P. Li, B. Feng, H. Wang, P. W. Tooley, and X. Zhang, *J. Basic Microbiol.* **51**, 61 (2011).
- [55] R. N. Trigiano, *Plant Pathology Concepts and Laboratory Exercises* (CRC Press, Boca Raton, FL, 2007).
- [56] H. V. Silva-Rojas, S. P. Fernández-Pavía, C. Góngora-Canul, B. C. Macías-López, and G. D. Ávila-Quezada, *Rev. Mex. Fitopatol.* **27**, 134 (2009).
- [57] G. Gilardi, M. Baudino, M. Moizio, M. Pugliese, A. Garibaldi, and M. Gullino, *Crop Protection* **53**, 13 (2013).
- [58] C. D. Lorenz and R. M. Ziff, *Phys. Rev. E* **57**, 230 (1998).
- [59] J. Schmelzer, S. A. Brown, A. Wurl, M. Hyslop, and R. J. Blaikie, *Phys. Rev. Lett.* **88**, 226802 (2002).
- [60] R. Kenna and B. Berche, *J. Phys. A: Math. Theor.* **50**, 235001 (2017).
- [61] B. Roy and S. Santra, *Physica A* **492**, 969 (2018).

Site-bond percolation solution to preventing the propagation of *Phytophthora* zoospores on plantations

J. E. Ramírez ^{1,2,*} C. Pajares,^{1,2} M. I. Martínez ³ R. Rodríguez Fernández ² E. Molina-Gayosso ⁴,
J. Lozada-Lechuga ⁴ and A. Fernández Téllez³

¹Departamento de Física de Partículas, Universidad de Santiago de Compostela, E-15782 Santiago de Compostela, España

²Instituto Galego de Física de Altas Enerxías, Universidad de Santiago de Compostela, E-15782 Santiago de Compostela, España

³Facultad de Ciencias Físico Matemáticas, Benemérita Universidad Autónoma de Puebla,
Apartado Postal 165, 72000 Puebla, Puebla, México

⁴Universidad Politécnica de Puebla, Tercer carril del Ejido Serrano, 72640, Juan C. Bonilla, Puebla, México



(Received 10 September 2019; accepted 30 January 2020; published 5 March 2020)

We propose a strategy based on the site-bond percolation to minimize the propagation of *Phytophthora* zoospores on plantations, consisting in introducing physical barriers between neighboring plants. Two clustering processes are distinguished: (i) one of cells with the presence of the pathogen, detected on soil analysis, and (ii) that of diseased plants, revealed from a visual inspection of the plantation. The former is well described by the standard site-bond percolation. In the latter, the percolation threshold is fitted by a Tsallis distribution when no barriers are introduced. We provide, for both cases, the formulas for the minimal barrier density to prevent the emergence of the spanning cluster. Though this work is focused on a specific pathogen, the model presented here can also be applied to prevent the spreading of other pathogens that disseminate, by other means, from one plant to the neighboring ones. Finally, the application of this strategy to three types of commercially important Mexican chili plants is also shown.

DOI: [10.1103/PhysRevE.101.032301](https://doi.org/10.1103/PhysRevE.101.032301)

I. INTRODUCTION

The genus *Phytophthora* (from Greek, meaning *phyto*, “plant,” and *phthora*, “destroyer” [1–3]) is one of the most aggressive phytopathogens that attack the roots of plants and trees in every corner of the world. The diseases caused by exposition to *Phytophthora* generate tremendous economical losses in agronomy and forestry. For example, *Phytophthora capsici* cause considerable damage in plantations of chili, cucumber, zucchini, etc. [4–6]. The same occurs with tomato and potato plantations, which are affected by *Phytophthora infestans* [7–9]. *Phytophthora cinnamomi* harms avocado plantations [10–12] and, together with *Phytophthora cambivora*, produce the ink disease, which is widely distributed in Europe [13–15]. *Phytophthora* has caused significant devastation on Galician chestnut and the Australian eucalypt, putting them close to extinction [16–18].

From a biological perspective, *Phytophthora* shares morphological characteristics with true fungi (Eumycota) such as mycelial growth or the dispersion of spores of mitotic or asexual origin. Its form of locomotion, by means of flagella [19], is a distinctive feature that enables them to have a great impact on the plant kingdom as phytopathogens. They can disperse through soil moisture or water films, including those on the surface of the plants. These motile zoospores, emerging from mature sporangia in quantities of 20 to 40, can swim chemotactically toward the plants [19–21]. When they reach the surface of the roots they lose their flagella,

and form a germination tube through which they penetrate the surface of the plant [22,23]. Moreover, many species of *Phytophthora* can persist as saprophytes if the environmental conditions are not appropriate but become parasitic in the presence of susceptible hosts [21]. Due to the physiology of the oomycetes most fungicides have no effect on them [1,24,25]. Therefore, research on nonchemical strategies that minimize or eliminate the propagation of the pathogen is necessary.

It has been noted that for some type of plants not all individuals manifest the disease after the exposition to a specific pathogen. We take advantage of this fact to define the pathogen susceptibility (χ) of a plant type as the fraction of individuals that get the disease. It can be interpreted as the probability that a sample of the plant gets sick after being exposed to the pathogen and can be measured in a laboratory or a greenhouse under controlled conditions or by direct observation in the plantation.

On the other hand, one of the models widely used to describe physical processes is the site-bond percolation, which has been applied to study the spread of diseases [26–29]. It is a generalization of the site and bond percolation that consists in determining both site and bond occupation probabilities needed to the emergence of a spanning cluster of sites connected by bonds. In this context, two nearest-neighboring sites do not belong to the same cluster if there is not a bond connecting them. In this work, occupied sites in the percolation system represent susceptible plants through which the propagation process can occur, and bonds represent the direction of propagation of the pathogen.

*jerc.fis@gmail.com

It is worth mentioning that zoospores move directly to neighboring plants. Placing physical barriers between them (that is, perpendicularly to the direction of propagation) can help to decrease the opportunity for root to root pathogen transmission. For instance, the Australian government recommends using physical root barriers such as impermeable membranes made of high-density polyethylene [30–33], which have been used in agriculture and horticulture. Trenches filled with compost (a mixture of manure and crop residues) in addition with biological control agents (for example, *Trichoderma spp.* or *Bacillus spp.*) could be used as a good barrier against soil-borne pathogens like oomycetes and fungi [34–36]. With the use of barriers it could be possible to fragment the spanning cluster of susceptible plants, preventing the propagation of the pathogen. Thus, if the pathogen susceptibility of the plant is known, then one can try to determine the minimal density of barriers (p_w) that stops the propagation of the pathogen. However, this density does not necessarily correspond to the bond percolation threshold.

Although this paper is motivated by the important problem caused by the propagation of *Phytophthora*, which is still unsolved nowadays, the strategy presented here can be adapted to mitigate the spread of other diseases. There exist other phytopathogens relevant to agronomy that disseminate over neighboring plants (for example by walking [37], rain splashing [38–40] or swimming [41]) like red spider mites, leaf rust and *Pythium* (with similar propagation mechanisms as *Phytophthora*), among others. In practice one only needs to find a suitable physical barrier that efficiently avoids nearest-neighbor propagation of the specific phytopathogen.

In Sec. II, we introduce the site-bond percolation model for the pathogen-plant interaction and the role of the barriers. Section III describes the simulation method used in this work and provides the simulation rules for the clustering process. It also shows an example of the simulation process and describes the data analysis method. In Sec. IV, we report the critical curves as a function of the initial percentage of inoculated soil for the barrier-free case. These curves indicate the maximum value of the pathogen susceptibility that guarantees a spanning cluster of diseased plants is not formed even if the soil is completely infested with the pathogen. Additionally, we provide the empirical formulas to determine the density of barriers that prevents the emergence of the spanning cluster when the susceptibility exceeds the aforementioned critical value. In Sec. V, we show the application of this method to three varieties of Mexican chili plants with high commercial value. Finally, Sec. VI presents the conclusions of this work.

II. MODEL

The plantation is modeled as a simple two-dimensional lattice (square, triangular, and honeycomb) wherein each site represents a plant. The lattice spacing is chosen as the maximum displacement length that the pathogen can travel before entering a state of dormancy or before dying due to starvation. This condition ensures the pathogen can only move to the nearest-neighbor cells as depicted in Fig. 1. We assume a site with an active pathogen will propagate the disease to all nearest-neighbor sites.

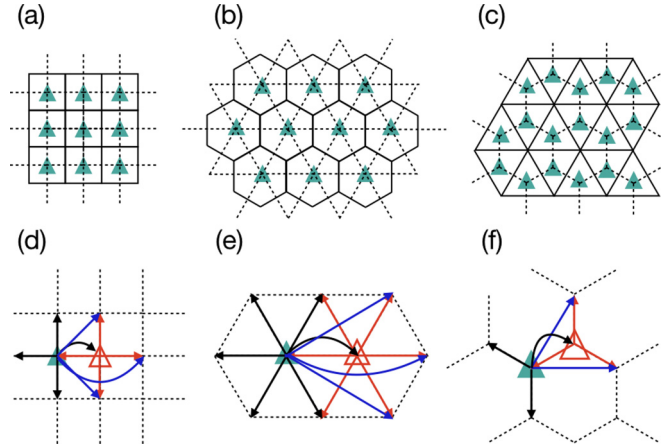


FIG. 1. Possible barrier locations (solid lines), directions of microorganism propagation (dotted lines), and modification of the nearest-neighbor meaning induced by inoculated cells with a resistant plant in square [(a) and (d)], triangular [(b) and (e)], and honeycomb [(c) and (f)] lattices. Bottom figures show susceptible plants (green triangle) with a neighboring resistant plant in an inoculated cell (red triangle). As a consequence of the microorganism propagation (red arrows), the nearest-neighbor definition (black arrows) is modified since the site with the susceptible plant can now be linked to farther sites (blue arrows).

Here the pathogen susceptibility plays an important role since resistant plants can act as a natural barrier for susceptible plants by locally containing the propagation process, i.e., a resistant plant does not disseminate the disease. In our model resistant plants are uniformly distributed on the system since it is not possible to determine in advance which seeds will grow into resistant or susceptible plants. In this way the pathogen susceptibility plays the role of the occupation probability in the traditional treatment of percolation theory.

Another essential variable that needs to be considered is the initial fraction of inoculated cells at the beginning of the propagation process which is denoted by I . In our model these cells are distributed uniformly over the lattice. This parameter is relevant to amalgamate adjacent-disjoint clusters promoting a favorable environment for the formation of a spanning cluster of diseased plants or of cells with the presence of the pathogen [42]. Additionally, we put barriers that are randomly distributed in the lattice. These are placed perpendicularly to the direction of propagation of the pathogen (see Fig. 1), and its primary function is to prevent the pathogen from reaching neighbor sites. Note that all possible barriers that can be placed form the dual lattice to that formed by all possible directions of propagation of the pathogen. Then the question we want to answer is as follows: What is the minimal barrier density, in terms of χ and I , that guarantees a spanning cluster will not appear?

We distinguish two different clustering processes: (i) the formation of clusters of cells with the presence of the pathogen and (ii) the formation of clusters of diseased plants. Although both processes are consequence of the propagation of the pathogen they depend in different ways on the intrinsic properties of the plants. In practice one would observe the first process if a pathogen soil test is performed while a visual

inspection of the damage on the plantation would reveal the second process. In the following we refer to them as *soil* and *plant* cases, respectively, and the corresponding variables will be labeled with a superscript.

In the soil case, for a lattice with N sites, the mean number of available plants $\langle N \rangle_{\text{av}}$ to the propagation process is $\langle N \rangle_{\text{av}} = N\chi$. Since the susceptibility of the plant and the inoculation state of the cell are independent variables, it is necessary to take into account the mean number of inoculated cells $\langle N \rangle_{\text{in}}$ with a resistant plant. This condition adds $\langle N \rangle_{\text{in}} = N(1 - \chi)I$ extra available cells. Thus, the total mean number of cells where the propagation process can occur is $\langle N \rangle_{\text{tot}} = \langle N \rangle_{\text{av}} + \langle N \rangle_{\text{in}}$. Therefore, the propagation takes place in a percolating system with an effective occupation probability $p_{\text{eff}}^{\text{soil}} = I + (1 - I)\chi$. In this case, the spanning cluster emerges if $p_{\text{eff}}^{\text{soil}} \geq p_{\text{cs}}$, where p_{cs} is the critical probability in the purely site percolation. Thus the desired percolation threshold is $p_{\text{eff}}^{\text{soil}} = p_{\text{cs}}$.

The introduction of barriers in the soil case makes the system suitable to be modeled with the site-bond percolation. The critical curves as a function of the occupation probabilities of sites (p_s) and bonds (p_b) has been empirically fitted using [43] $p_b = B/(p_s + A)$, where $A = (p_{\text{cb}} - p_{\text{cs}})/(1 - p_{\text{cb}})$, $B = p_{\text{cb}}(1 - p_{\text{cs}})/(1 - p_{\text{cb}})$, and p_{cb} is the critical probability in the purely bond percolation. Moreover, since barriers are located in the dual lattice, the density of barriers and the bond occupation probability are related by $p_b + p_w^{\text{soil}} = 1$, that is, the joint set of barriers and bonds it is exactly \mathcal{N}_b (see Sec. III). So we finally find that the critical curves for the soil case can be written as

$$p_w^{\text{soil}} = 1 - \frac{p_{\text{cb}}(1 - p_{\text{cs}})}{(1 - p_{\text{cb}})(I + (1 - I)\chi) + p_{\text{cb}} - p_{\text{cs}}}. \quad (1)$$

On the other hand, for the plant case, inoculated cells with a resistant plant do not belong to the cluster of diseased plants. However, these cells play an essential role since adjacent-disjoint clusters can be amalgamated through them. This fact modifies the nearest-neighbor meaning since it is then possible to link two susceptible plants separated by a distance greater than the lattice spacing (see Fig. 1), then the possibility to amalgamate adjacent-disjoint clusters is increased [42].

The main difference between the soil and plant cases is just this amalgamating role played by inoculated cells with a resistant plant at the beginning of the propagation process. In the soil case, these cells are considered as occupied sites, while in the plant case, they do not belong to any cluster; however, they can transmit the disease over neighboring susceptible plants. Schematically, this latter situation looks like a healthy plant with sick neighbors.

III. SIMULATION METHOD

We implemented a modified version of the Newman-Ziff algorithm reported in Refs. [44,45] to determine the percolation threshold.

Since the susceptibility condition of each plant and the cells' inoculation state are independent of each other they are stored in separate matrices in the simulation. These matrices, that we call \mathbb{X} and \mathbb{I} , respectively, are initially null. They

are then filled according to the predefined values of χ and I . For the case with no barriers, however, only the knowledge of the inoculated cells is required to determine the percolation thresholds.

For simplicity we describe the implementation of the algorithm for a square lattice. However, this algorithm can also be used for other lattices simply changing the implementation of the nearest-neighbor definition.

Each cell of the $L \times L$ matrices \mathbb{X} and \mathbb{I} is labeled with a progressive number $M = iL + j$, for the cell at row i and column j . The set of cells' labels is then $\mathcal{N} = \{0, 1, 2, \dots, L^2 - 1\}$. On the other side, the possible propagation directions for all cells form a network with $2L(L - 1)$ bonds since the system is considered as free of periodic boundary conditions. As we did with the cells, each bond is labeled with progressive numbers that form the set $\mathcal{N}_b = \{0, 1, 2, \dots, 2L(L - 1) - 1\}$.

An initial number of inoculated cells n_I is drawn from the binomial distribution $B(L^2, I)$ and then n_I labels are randomly taken from the set \mathcal{N} . The corresponding cells are the sites from which the infection process will propagate. These cells are marked by changing their state from 0 to 1. The initial distribution of susceptible plants, that is, plants that will get the disease if they are exposed to the pathogen, is obtained in a similar way. Note that only the initial conditions are set so far and the propagation process has not been started so that no cells are linked yet.

To add bonds between cells the \mathcal{N}_b labels are randomly permuted and then the corresponding bonds are added one at a time until a spanning cluster is formed. It should be recalled that bonds determine the direction of propagation in this model.

To decide which bonds will connect the sites we impose rules based on the way the pathogen transports itself from site to site. Since the zoospores are capable of detecting the presence of neighboring plants, they will swim toward them as soon as they emerge from the sporangia. If a zoospore reaches a resistant plant, then it will either enter a latency state or die from inanition so that it will not be able to further propagate the disease. If, on the other hand, the zoospore arrives at a susceptible plant, then it will attack the plant and produce new sporangia. They, in turn, will produce new zoospores that will eventually swim toward neighboring plants. Thus the rules can be stated as follows.

A bond will connect two nearest-neighbor sites if:

- (1) Soil case:
 - (a) Any of the sites was inoculated during the initial configuration.
 - (b) Both sites have susceptible plants.
- (2) Plant case:
 - (a) Any of the sites was inoculated during the initial configuration and the other has a susceptible plant.
 - (b) Both sites have susceptible plants.

This way bonds are added one by one, and sites are connected according to the rules above, until a cluster that connects one side of the lattice to the opposite one, the so-called spanning cluster, appears. The union-find algorithm is used to connect sites. Since not every site pair can interact not every bond can connect adjacent sites. In order to identify the spanning cluster, before starting the simulation process, susceptible plants in the last and first rows are united with

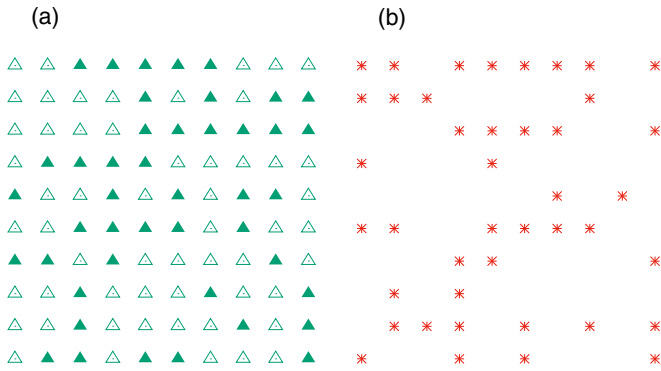


FIG. 2. Examples of possible initial configurations of a system of size $L = 10$. (a) Distribution of cells with susceptible (filled triangles) and resistant (empty triangles) plants. (b) Distribution of inoculated cells.

auxiliary labels -1 and -2, respectively. Then, the simulation process is stopped when the labels $\{-1,-2\}$ change to the same value.

The essential difference between the two cases is the role played by the inoculated cells with a resistant plant. In the soil case they become occupied sites while in the plant case they may merge disjoint clusters.

To visualize the difference between both cases consider an $L = 10$ system with $\chi = 0.5$ and $I = 0.4$. Figure 2 shows one possible initial configuration of susceptible plants and inoculated cells before the propagation process starts.

In a system of size $L = 10$ there are 180 bonds. A possible random permutation of their labels is listed below:

{118, 63, 26, 119, 160, 22, 64, 142, 156, 126, 8, 152, 73, 127, 32, 78, 81, 170, 36, 92, 89, 123, 57, 68, 12, 33, 24, 129, 158, 46, 169, 82, 48, 147, 69, 38, 18, 56, 168, 178, 179, 164, 114, 6, 79, 42, 86, 41, 13, 52, 165, 115, 43, 85, 172, 116, 133, 11, 27, 139, 29, 15, 0, 138, 122, 40, 7, 148, 74, 71, 113, 177, 111, 135, 37, 51, 67, 9, 121, 98, 99, 35, 49, 108, 151, 53, 173, 39, 1, 5, 2, 153, 45, 146, 76, 59, 145, 143, 163, 96, 16, 104, 101, 61, 144, 28, 102, 17, 88, 31, 3, 141, 109, 77, 65, 80, 166, 106, 167, 117, 70, 130, 21, 83, 140, 20, 157, 10, 136, 161, 137, 107, 100, 150, 110, 91, 132, 128, 112, 93, 44, 149, 19, 94, 131, 154, 155, 30, 62, 171, 23, 34, 55, 4, 54, 176, 58, 75, 174, 50, 60, 125, 47, 25, 103, 134, 120, 159, 90, 84, 14, 87, 175, 124, 95, 105, 66, 72, 97, 162}.

The bonds are added in this order until a spanning cluster appears. The entries of one of the cells a given bond can connect are given by $i = \lfloor h/(2L - 1) \rfloor$ and $j = h \bmod (2L - 1)$, where h is the bond's label and $\lfloor x \rfloor$ denotes the integer part of x . Note that the orientation of the bond is identified as horizontal if $j < L - 2$ or vertical otherwise. In addition, the value of j should be corrected for vertical bonds by subtracting $L - 1$. Then the cells with entries i, j and $i, j + 1$ are taken if the bond is horizontal; while the cells at i, j and $i + 1, j$ are taken if the bond is vertical. Finally, if the pair taken fulfills the rules given previously, then they are connected using the union-find algorithm.

Figure 3 shows the networks formed by connected bonds in both cases. While in the soil case 121 bonds were added before the spanning cluster appeared, in the plant case were

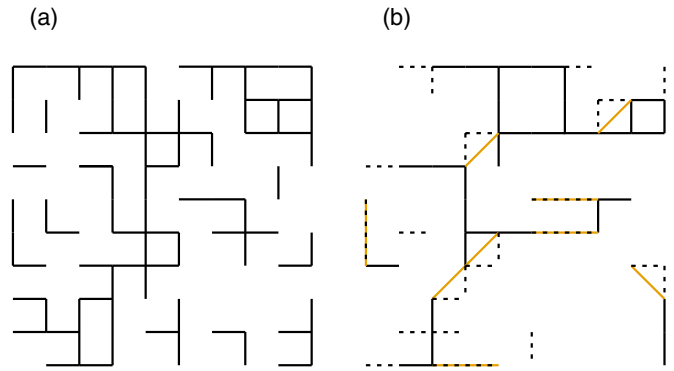


FIG. 3. Spanning clusters formed in the (a) soil and (b) plant cases for the initial conditions of Fig. 2 and the list of bonds given in the text. Only the bonds that connect sites are shown (black lines). In the case (b), bonds connecting a resistant plant in an inoculated site to a susceptible plant are represented with dashed lines. Yellow lines show the modification of the nearest-neighbor definition.

needed 160 bonds. Note that, although each network has its own topology, in the plant case the fundamental role for the formation of a spanning cluster is played by the modification of the nearest-neighbor definition [yellow lines in Fig. 3(b)] introduced by the interactions between susceptible plants and inoculated cells with a resistant plant on it [dashed lines in Fig. 3(b)]. This clearly shows the consequence of this type of interactions, namely their capacity to merge disjoint clusters of susceptible plants.

Data analysis

Using this method, we determined the probability P_n that a spanning cluster appears after adding n bonds (or sites) [46] as an average over 10^4 runs for each pair (χ, I) . Starting in $\chi = 1$ and $I = 1$ we decreased their values independently in steps of $\Delta\chi = \Delta I = 0.05$. Then the percolation probability is computed as $P(p) = \sum_n B(N, n, p)P_n$, where $B(N, n, p)$ is the binomial distribution [44,45], N is the total number of sites or bonds in the lattice, and p is the occupation probability of sites or bonds correspondingly. Last, the percolation threshold is determined by solving the equation $P(p_c) = 0.5$ [47]. To this end, the percolation probability is computed from $\langle n_c \rangle / L^2 - 0.15$ to $\langle n_c \rangle / L^2 + 0.15$ in steps of $\Delta p = 0.01$. Then $P(p) = 0.5[1 + \tanh((p - p_c) / \Delta_L)]$ is fitted to the estimated data. Here p_c is the estimation of the percolation threshold and Δ_L is the width of the sigmoid transition [47].

To take finite-size effects into account we also performed simulations using the system size $L = 32, 64, 128, \text{ and } 256$. Thus the percolation threshold in the thermodynamic limit is estimated by the extrapolation of the scaling relation $p_c - p_c(L) \propto L^{-1/\nu}$, where ν is the exponent corresponding to the correlation length [48]. It is well known that the transition width Δ_L scales as a function of the system size L as $\Delta_L \propto L^{-1/\nu}$ [49]. From the fit of the percolation probability data, we found that $\nu = 4/3$, which is in good agreement with the results reported in the literature for the percolation theory in 2D. Finally, the critical density of barriers is calculated as $p_w = 1 - p_{cb}^*$, where p_{cb}^* is the bond percolation threshold as a function of χ and I .

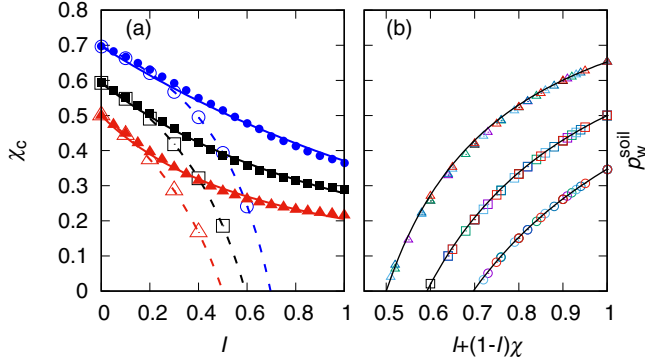


FIG. 4. (a) Critical curves for cluster formation over infested soil (hollow figures) and infected plants (solid figures) on triangular (triangles), square (squares), and honeycomb (circles) lattices with no barriers. Theoretical curves for the soil case (dashed lines) and the fit to the data for the plant case (continuous lines) are also shown. (b) Simulation (figures) and theoretical (lines) critical curves in the soil case for square (squares), triangular (triangles), and honeycomb (circles) lattices for several values of I : 0.0 (black), 0.1 (purple), 0.2 (green), 0.3 (cyan), 0.4 (blue), and 0.5 (red).

IV. RESULTS

Simulation results for the critical curves of both soil and plant cases with no barriers are shown in Fig. 4(a). Notably, our results for χ_c^{soil} are very well described by the parametrization $p_{\text{eff}}^{\text{soil}} = I + (1 - I)\chi = p_{\text{cs}}$. Notice that the critical curves for χ_c^{plant} deviate from those for χ_c^{soil} for $I > 0.15$. This is due to nonsusceptible plants lying in inoculated cells which do not belong to the clusters and can serve as a bridge between their adjacent sites. We found that χ_c^{plant} can be well fitted by the Tsallis distribution $p_{\text{cs}}/(1 + aI/n)^n$, with $a = 0.91 \pm 0.03$ and 1.40 ± 0.06 and $n = 2.0 \pm 0.4$ and 1.1 ± 0.1 for the square and triangular lattices, respectively. For the honeycomb lattice n takes a large value so we used $p_{\text{cs}} \exp(-aI)$ with $a = 0.63 \pm 0.01$. This behavior can be understood as the collective contribution of the interaction between susceptible plants and infected cells with a resistant plant. Note that the probability of observing this pair become higher as χ decreases and I increases, and thus, the percolating system looks like a lattice formed by regular sites and sites involving complex nearest neighbors. The main result of this analysis is the existence of a minimal susceptibility that guarantees the nonemergence of a spanning cluster of diseased plants even if all cells are inoculated, that is, the value of χ_c^{plant} for $I = 1$. However, if $\chi > \chi_c^{\text{soil}}$ or $\chi > \chi_c^{\text{plant}}$, then it is necessary to use the barrier strategy to reduce the connectedness of the lattice. In Fig. 4(b), we show the simulation results for the soil case. Notice that they are well described by Eq. (1), which corresponds to the description of the typical critical curves in the site-bond percolation with an occupation probability $p_{\text{eff}}^{\text{soil}}$. This is because in this case the infected cells are taken into account in the cluster formation process even if the plant does not become sick.

On the other hand we found, for the plants case, that the relation among χ , χ_c^{plant} , and p_w^{plant} is given by the power law $(\chi - \chi_c^{\text{plant}}) = \alpha(p_w^{\text{plant}} \chi / \chi_c^{\text{plant}})^{\beta}$ when I is fixed, as it is

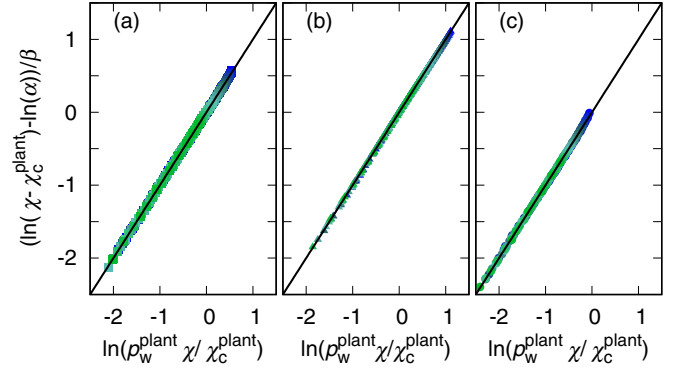


FIG. 5. Power-law relation among χ , χ_c^{plant} , and p_w^{plant} in the plant case when I is fixed for (a) square, (b) triangular, and (c) honeycomb lattices. Black solid line is the identity function. The color scale indicates the value of I from $I = 0$ (green) up to $I = 1$ (blue) in steps of $\Delta I = 0.05$.

shown in Fig. 5. It should be noted that both α and β depend on I . Particularly, β takes values between 0.95 and 1.18 for all lattices. Then, the critical curves for the plants case are given by

$$p_w^{\text{plant}} = \frac{\chi_c^{\text{plant}}}{\chi} \left(\frac{\chi - \chi_c^{\text{plant}}}{\alpha} \right)^{1/\beta}, \quad (2)$$

which matches very well the simulation data for the square, triangular, and honeycomb lattices as shown in Fig. 6 for different values of I . Table I shows the values of the parameters α and β (for different values of I) given by the fit to simulation data for the square, triangular, and honeycomb lattices. Moreover, in the case $\chi = 1$, $p_w^{\text{plant}} = 1 - p_{\text{cb}}$ as expected since, under this condition, the system corresponds to the traditional bond percolation model.

V. APPLICATION TO CHILI PLANTATIONS

Application of Eq. (2) requires the knowledge of the plant's pathogen susceptibility. This quantity has been measured experimentally as described in Ref. [42]. In general terms their method consists in sowing plants in previously sterilized soil and inoculating a fraction of the substrate with oomycetes. The pathogen is then allowed to propagate through the plantation and the presence of the pathogen is assessed for each plant. The ratio of the number of live infected plants to the total number of infected plants gives the surviving rate \mathcal{P} . The pathogen susceptibility of the plant is then calculated as $\chi = 1 - \mathcal{P}$.

The reported values of the pathogen susceptibility for the varieties arbol, poblano, and serrano plants of chilis (which are of high commercial value in Mexico) are 1.00, 0.89, and 0.60, respectively. Putting these values into Eq. (2) we obtained the curves for p_w^{plant} as a function of I shown in Fig. 7 for a square lattice. Note that as the value of χ approaches 1, like for the arbol and poblano chilis, the barrier density approaches the bond percolation threshold ($p_{\text{cb}} = 0.5$) since in these particular cases the percolating system is very similar to the bond percolation model. On the other side, as χ

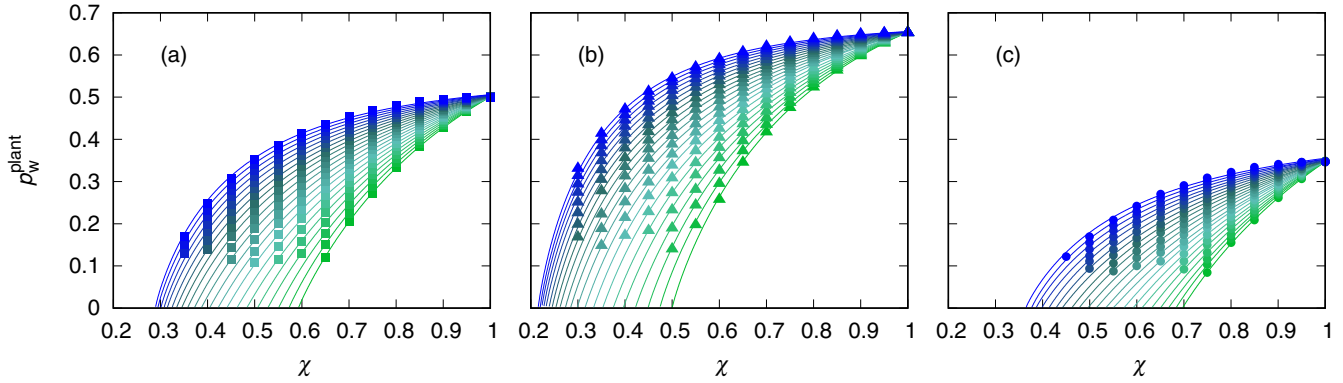


FIG. 6. Comparison between simulation results (figures) for p_w^{plant} as a function of the susceptibility and the curve proposed in Eq. (2) (solid lines) for (a) square, (b) triangular, and (c) honeycomb lattices. The color scale indicates the value of I from $I = 0$ (green) up to $I = 1$ (blue) in steps of $\Delta I = 0.05$.

approaches the site percolation threshold, like for the serrano chili, the range of possible values for p_w^{plant} becomes larger; however, $p_w^{\text{plant}}(I = 1) \approx 0.41$ is less than 0.5. In practice, this means an 18% less barriers are needed to prevent the disease propagation.

Also as χ becomes less and less than p_{cs} , the value of p_w^{plant} decreases until it vanishes. This point, when $p_w^{\text{plant}}(I = 1) = 0$, corresponds to the intersection of the critical χ_c^{plant} curve with the vertical line $I = 1$ (see Fig. 4). This is just the greatest value of a plant's susceptibility that makes the barrier strategy unnecessary.

TABLE I. Fit parameters for the square (\square), triangular (Δ), and honeycomb (\circ) lattices. Error estimates in the last significant figure are indicated in parentheses.

I	α_{\square}	β_{\square}	α_{Δ}	β_{Δ}	α_{\circ}	β_{\circ}
0.00	0.4870(9)	1.065(3)	0.3685(5)	1.132(5)	0.621(5)	1.031(8)
0.05	0.4922(8)	1.050(3)	0.3689(5)	1.099(5)	0.637(2)	1.032(3)
0.10	0.4956(6)	1.029(2)	0.3673(4)	1.077(3)	0.636(2)	1.001(3)
0.15	0.4982(5)	1.013(2)	0.3646(4)	1.051(3)	0.657(3)	1.003(5)
0.20	0.5000(4)	1.005(2)	0.3598(4)	1.032(3)	0.669(3)	0.996(5)
0.25	0.4994(2)	0.994(1)	0.3530(2)	1.029(1)	0.674(2)	0.974(4)
0.30	0.4977(3)	0.990(1)	0.3445(1)	1.024(1)	0.685(2)	0.974(3)
0.35	0.4941(4)	0.989(2)	0.334(1)	1.023(6)	0.698(3)	0.980(5)
0.40	0.4892(3)	0.991(2)	0.3253(2)	1.022(1)	0.696(2)	0.954(3)
0.45	0.4821(3)	0.996(2)	0.3145(2)	1.025(1)	0.711(2)	0.979(4)
0.50	0.4741(2)	1.003(1)	0.3036(3)	1.033(2)	0.713(1)	0.982(2)
0.55	0.4653(2)	1.013(1)	0.2925(4)	1.047(2)	0.715(2)	0.987(4)
0.60	0.4551(2)	1.025(1)	0.2825(3)	1.052(2)	0.720(1)	1.005(3)
0.65	0.4450(1)	1.036(1)	0.2721(3)	1.066(2)	0.717(2)	1.016(4)
0.70	0.4342(3)	1.050(2)	0.2622(4)	1.080(2)	0.708(3)	1.014(8)
0.75	0.4235(5)	1.070(3)	0.2531(4)	1.094(2)	0.705(3)	1.037(7)
0.80	0.4120(6)	1.082(4)	0.2442(4)	1.107(2)	0.699(4)	1.057(9)
0.85	0.4017(8)	1.104(5)	0.2361(5)	1.122(3)	0.687(5)	1.06(1)
0.90	0.391(1)	1.123(7)	0.2285(5)	1.137(2)	0.676(5)	1.08(2)
0.95	0.380(1)	1.142(8)	0.2216(6)	1.152(3)	0.669(5)	1.11(2)
1.00	0.371(1)	1.163(9)	0.2148(7)	1.165(4)	0.654(6)	1.12(2)

VI. CONCLUSIONS

In summary, we have presented a strategy based on the site-bond percolation model to prevent the propagation of *Phytophthora* over a plantation. This strategy consists of placing barriers between adjacent cells, whose density depends on χ and I . Two different clustering processes were analyzed: (i) clusters of cells with the presence of the pathogen and (ii) clusters of diseased plants. The former is related to a soil test and the latter to a direct visual inspection of the damage on the plantation. It was found that both processes are indistinguishable, and therefore described by the same critical curve, for $I < 0.15$. On the contrary, for $I > 0.15$ this behavior does not hold and different approaches for each process are necessary. Differences in the critical density of barriers between the *soil* and *plant* cases are a consequence of the hybridization process of the lattice, which leads to a major deviation when I increases and χ decreases (see Fig. 6). The soil case is

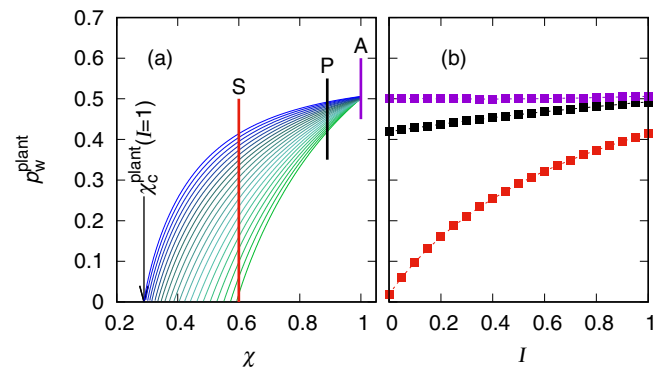


FIG. 7. (a) Critical values p_w^{plant} for arbol (A), poblano (P), and serrano (S) chili plants sowed with a square lattice arrangement. Vertical lines indicate their susceptibilities: 1.00 (A), 0.89 (P), and 0.60 (S). The solid curves are the same as in Fig. 6. $\chi_c^{\text{plant}}(I = 1) = 0.28883 \pm 0.00007$ is the maximum value of a plant's susceptibility that inhibits the formation of a cluster of diseased plants, even in the extreme case where the pathogen is present all over the plantation. (b) Values of p_w^{plant} given by Eq. (2) and data from Table I for the arbol (purple), poblano (black), and serrano (red) chili plants on a square lattice.

described by the site-bond percolation model with an effective occupation probability given by $p_{\text{eff}}^{\text{soil}} = I + (1 - I)\chi$. Then the critical curves are as usual [see Eq. (1)] because the clustering process of the infected cells does not distinguish the sickness states of the plant.

In the plant case, the critical curves predict the existence of a minimal susceptibility χ_c^{plant} that guarantees a spanning cluster of infected plants will not appear, that is, if $\chi < \chi_c^{\text{plant}}$ even when $p_w = 0$ and $I = 1$. Values for the minimal susceptibility in square, triangular, and honeycomb lattices were found to be 0.28883 ± 0.00007 , 0.2141 ± 0.0003 , and 0.364 ± 0.003 , respectively. Particularly, for the square lattice, this value is in agreement with the critical probability of lattices with more complex neighborhoods [50,51].

Based on the obtained results, we would advise farmers and agronomists either to sow types of plants having a pathogen susceptibility lower than χ_c^{plant} or to apply the barriers strategy with a barrier density given by Eq. (2). A very important advantage of this strategy is that it does not require to remove plants therefore avoiding deforestation.

This strategy could be verified under controlled conditions, for example, in greenhouses, tree nurseries, and hydroponics,

where *Phytophthora* and other phytopathogens cause great devastation. On the other hand, its application on a real-life situation requires us to take into account other ecological and environmental variables, such as plant-plant or (beneficial) microorganism-plant interactions, irrigation system, spatial distribution of plants, the care provided by the farmer or the possibility of having more than one type of pathogen in the same parcel of soil.

Finally, Eq. (2) for $I = 0$ could be used as an alternative parametrization of the critical curves in the site-bond percolation model even for lattices defined in dimensions higher than two.

ACKNOWLEDGMENTS

J.E.R. acknowledges financial support from CONACyT (postdoctoral fellowship Grant No. 289198). C.P. was supported by the grant Maria de Maeztu Unit of Excellence MDM-20-0692 and FPA Project No. 2017-83814-P of Ministerio de Ciencia, Innovación y Universidades (Spain), FEDER, and Xunta de Galicia.

-
- [1] D. C. Erwin and O. K. Ribeiro, *Phytophthora Diseases Worldwide* (American Phytopathological Society, MN, 1996).
- [2] D. Shaw, *J. Agr. Sci.* **131**, 245 (1998).
- [3] T. Reglinski, M. Spiers, J. Taylor, and M. Dick, *N. Z. J. Forest.* **54**, 16 (2010).
- [4] F. J. Polach and R. K. Webster, *Phytopathology* **62**, 20 (1972).
- [5] M. K. Hausbeck and K. H. Lamour, *Plant Dis.* **88**, 1292 (2004).
- [6] K. H. Lamour, R. Stam, J. Jupe, and E. Huitema, *Mol. Plant Pathol.* **13**, 329 (2012).
- [7] H. Lozoya-Saldaña, M. N. Robledo-Esqueda, P. Rivas-Valencia, S. Sandoval-Islas, M. T. Beryl Colinas y León, and C. Nava-Díaz, *Rev. Chap. Ser. Hortic.* **23**, 175 (2017).
- [8] S. K. Shakya, M. M. Larsen, M. M. Cuenca-Condoy, H. Lozoya-Saldaña, and N. J. Grünwald, *Plant Dis.* **102**, 1534 (2018).
- [9] B. J. Haas *et al.*, *Nature* **461**, 393 (2009).
- [10] G. Weste and G. C. Marks, *Annu. Rev. Phytopathol.* **25**, 207 (1987).
- [11] M. You and K. Sivasithamparam, *Appl. Soil Ecol.* **2**, 33 (1995).
- [12] H. S. Judelson and B. Messenger-Routh, *Phytopathology* **86**, 763 (1996).
- [13] A. Vannini and A. M. Vettraino, *For. Snow Landsc. Res.* **76**, 345 (2001).
- [14] A. M. Vettraino, O. Morel, C. Perlerou, C. Robin, S. Diamandis, and A. Vannini, *Eur. J. Plant Pathol.* **111**, 169 (2005).
- [15] A. Vannini, G. Natili, N. Anselmi, A. Montagni, and A. M. Vettraino, *Forest Pathol.* **40**, 73 (2010).
- [16] E. Vieitez, *Botanica Complutensis* **11**, 25 (1981).
- [17] M. V. González, B. Cuenca, M. López, M. J. Prado, and M. Rey, *Sci. Hortic.* **130**, 459 (2011).
- [18] M. Miranda-Fontaina, J. Fernández-López, A. Vettraino, and A. Vannini, *Silvae Genet.* **56**, 11 (2007).
- [19] D. C. Erwin and O. K. Ribeiro, *Phytophthora Diseases Worldwide* (American Phytopathological Society, Minneapolis, 1996).
- [20] E. Bernhardt and R. Grogan, *Phytopathology* **72**, 507 (1982).
- [21] A. R. Hardham, *Mol. Plant Pathol.* **6**, 589 (2005).
- [22] B. Feng, P. Li, H. Wang, and X. Zhang, *Microb. Pathogen.* **49**, 23 (2010).
- [23] P. Li, B. Feng, H. Wang, P. W. Tooley, and X. Zhang, *J. Basic Microb.* **51**, 61 (2011).
- [24] Y. Cohen and M. D. Coffey, *Annu. Rev. Phytopathol.* **24**, 311 (1986).
- [25] A. Drenth and D. I. Gest, in *Diversity and Management of Phytophthora in Southeast Asia*, edited by A. Drenth and D. I. Gest (ACIAR, Canberra, 2004), Vol. 114, pp. 30–41 and 154–160.
- [26] H. L. Frisch and J. M. Hammersley, *J. Soc. Ind. Appl. Math.* **11**, 894 (1963).
- [27] D. S. Callaway, M. E. J. Newman, S. H. Strogatz, and D. J. Watts, *Phys. Rev. Lett.* **85**, 5468 (2000).
- [28] M. E. J. Newman, *Phys. Rev. E* **66**, 016128 (2002).
- [29] N. Madar, T. Kalisky, R. Cohen, D. ben Avraham, and S. Havlin, *Eur. Phys. J. B* **38**, 269 (2004).
- [30] W. A. Dunstan, T. Rudman, B. L. Shearer, N. A. Moore, T. Paap, M. C. Calver, R. Armistead, M. P. Dobrowolski, B. Morrison, K. Howard, E. O’Gara, C. Crane, B. Dell, P. O’Brien, J. A. McComb, and G. E. S. J. Hardy, Research into natural and induced resistance in Australian native vegetation of *Phytophthora cinnamomi* and innovative methods to contain and/or eradicate within localised incursions in areas of high biodiversity in Australia, Technical Report No. 19/2005DEH, Centre for *Phytophthora* Science and Management, Western Australia, 2008.

- [31] C. P. Dunne, C. E. Crane, M. Lee, T. Massenbauer, S. Barrett, S. Comer, G. J. Freebury, D. J. Utber, M. J. Grant, and B. L. Shearer, *N. Z. J. Forest. Sci.* **41**, S121 (2011).
- [32] W. A. Dunstan, T. Rudman, B. L. Shearer, N. A. Moore, T. Paap, M. C. Calver, B. Dell, and G. E. S. J. Hardy, *Biol. Invas.* **12**, 913 (2011).
- [33] B. L. Shearer, C. E. Crane, R. G. Fairman, M. J. Dillon, and R. M. Buehrig, *Australas. Plant Path.* **43**, 327 (2014).
- [34] G. Bonanomi, V. Antignani, C. Pane, and F. Scala, *J. Plant Pathol.* **89**, 311 (2007).
- [35] H. A. J. Hoitink, L. V. Madden, and A. E. Dorrance, *Phytopathology* **96**, 186 (2006).
- [36] C. M. Craft and E. B. Nelson, *Appl. Environ. Microb.* **62**, 1550 (1996).
- [37] C. E. M. van, den Boom, T. A. van Beek, and M. Dicke, *J. Appl. Entomol.* **127**, 177 (2003).
- [38] L. Geagea, L. Huber, I. Sache, D. Flura, H. McCartney, and B. Fitt, *Agr. Forest Meteorol.* **101**, 53 (2000).
- [39] S. Saint-Jean, A. Testa, L. Madden, and L. Huber, *Agr. Forest Meteorol.* **141**, 257 (2006).
- [40] T. Gilet and L. Bourouiba, *Integr. Comp. Biol.* **54**, 974 (2014).
- [41] C. A. Walker and P. van West, *Fungal Biol. Rev.* **21**, 10 (2007).
- [42] J. E. Ramírez, E. Molina-Gayosso, J. Lozada-Lechuga, L. M. Flores-Rojas, M. I. Martínez, and A. Fernández Téllez, *Phys. Rev. E* **98**, 062409 (2018).
- [43] Y. Y. Tarasevich and S. C. van der Marck, *Int. J. Mod. Phys. C* **10**, 1193 (1999).
- [44] M. E. J. Newman and R. M. Ziff, *Phys. Rev. Lett.* **85**, 4104 (2000).
- [45] M. E. J. Newman and R. M. Ziff, *Phys. Rev. E* **64**, 016706 (2001).
- [46] S. Mertens and C. Moore, *Phys. Rev. E* **86**, 061109 (2012).
- [47] M. D. Rintoul and S. Torquato, *J. Phys. A-Math. Gen.* **30**, L585 (1997).
- [48] D. Stauffer and A. Aharony, *Introduction to Percolation Theory* (Taylor & Francis, London, 2014).
- [49] A. Coniglio, *J. Phys. A-Math. Gen.* **15**, 3829 (1982).
- [50] K. Malarz and S. Galam, *Phys. Rev. E* **71**, 016125 (2005).
- [51] M. Majewski and K. Malarz, *Acta Phys. Pol. B* **38**, 2191 (2007).

Percolation-intercropping strategies to prevent dissemination of phytopathogens on plantations



Cite as: Chaos 31, 063105 (2021); doi: 10.1063/5.0044714

Submitted: 18 January 2021 · Accepted: 5 April 2021 ·

Published Online: 1 June 2021



Diana Rosales Herrera,¹ J. E. Ramírez,^{2,3,a)} M. I. Martínez,¹ H. Cruz-Suárez,¹ A. Fernández Téllez,¹
Jesús F. López-Olguín,² and Agustín Aragón García²

AFFILIATIONS

¹Facultad de Ciencias Físico Matemáticas, Benemérita Universidad Autónoma de Puebla, Apartado Postal 165, 72000 Puebla, Puebla, Mexico

²Centro de Agroecología, Instituto de Ciencias, Benemérita Universidad Autónoma de Puebla, Edificio VAL 1 - Ecomcampus Valsequillo, Km 1.7 carretera a San Baltazar Tetela, San Pedro Zacachimalpa, 72960, Puebla, Puebla, Mexico

³Departamento de Física de Partículas and Instituto Galego de Física de Altas Enerxías, Universidad de Santiago de Compostela, E-15782 Santiago de Compostela, Spain

^{a)}Author to whom correspondence should be addressed: jhony.ramirezcanino@viep.com.mx

ABSTRACT

Phytophthora is one of the most aggressive and worldwide extended phytopathogens that attack plants and trees. Its effects produce tremendous economical losses in agronomy and forestry since no effective fungicide exists. We propose to combine percolation theory with an intercropping sowing configuration as a non-chemical strategy to minimize the dissemination of the pathogen. In this work, we model a plantation as a square lattice where two types of plants are arranged in alternating columns or diagonals, and *Phytophthora* zoospores are allowed to propagate to the nearest and next-to-nearest neighboring plants. We determine the percolation threshold for each intercropping configuration as a function of the plant's susceptibilities and the number of inoculated cells at the beginning of the propagation process. The results are presented as phase diagrams where crop densities that prevent the formation of a spanning cluster of susceptible or diseased plants are indicated. The main result is the existence of susceptibility value combinations for which no spanning cluster is formed even if every cell in the plantation is sowed. This finding can be useful in choosing a configuration and density of plants that minimize damages caused by *Phytophthora*. We illustrate the application of the phase diagrams with the susceptibilities of three plants with a high commercial value.

Published under an exclusive license by AIP Publishing. <https://doi.org/10.1063/5.0044714>

The propagation of *Phytophthora* zoospores on plantations is modeled as a transport phenomenon on a percolation system wherein the occupied sites represent susceptible plants. In particular, we explore the effects of the disease spreading over intercropping plantation configurations (by sowing two different types of plants in alternate columns or diagonals). This ecofriendly strategy can be useful in choosing a configuration and density of plants that minimize damages caused by *Phytophthora* in situations where the control or the management of the plantation is not suitable for homogeneously distributed plants.

I. INTRODUCTION

Percolation theory is one of the most widely applied models in statistical physics,^{1,2} ranging from the study of the formation of galactic structures³ to the characteristics of the quark matter under extreme conditions.^{4,5} This theory was first proposed as a framework to explain transport phenomena that occur on porous media.⁶ In this theory, the porous media can be modeled as a square lattice, wherein each cell is independently assigned as occupied or empty with probability p and $1 - p$, respectively. Occupied sites are able to allow the flux of the transport phenomena. At a low occupation probability, there are only a few occupied sites. On the other hand, for high

occupation probability, almost all of the occupied sites are grouped in a big cluster that connects two opposite sides of the lattice, the so-called spanning cluster.^{2,7} In percolation theory, the fundamental question to answer is the following: What is the minimum occupation probability at which the spanning cluster emerges? This critical probability is the well-known percolation threshold.

The propagation of diseases can be modeled as a percolating process that occurs over a network connecting susceptible individuals.^{8–11} With the help of percolation theory, a better understanding of this problem has been reached, establishing the conditions to prevent the outbreak of some pathogens and diseases.^{12–14} Applications of percolation theory in agronomy and forestry are straightforward since traditional plantations can be modeled as simple regular lattices.^{15–22}

In agronomy and forestry, the genus *Phytophthora* (from Greek *phyto*, meaning “plant,” and *phthora*, “destroyer”^{23,24}) is considered one of the phytopathogens with the highest negative ecological impact due to the vast number of hosts that it attacks. *Phytophthora* species have presence all over the world. For instance, *P. cinnamomi* is found in the USA, Australia, and Western Europe, *P. cambivora* in south-east Europe, *P. katsurae* in Japan and South Korea, and *P. capsici* in Mexico.²⁵ The harm *Phytophthora* causes not only produce significant economic losses, but it has also caused ecological devastation in 15 biodiversity hotspots throughout the world, including the Mediterranean basin, south of Western Australia, and the fynbos of South Africa.²⁶ One of the main features that make *Phytophthora* a successful phytopathogen is its capability to move chemotactically toward the plants by using its flagella to swim in thin water films or soil moisture.^{23,27,28} Due to its physiology, this pathogen cannot be controlled with pesticides or fungicides.^{23,29,30} An alternative approach to prevent its propagation could be based on the modification of the sown configurations.

Some authors propose a well-mixed distribution of plants as a strategy to avoid the disease propagation.^{21,31} In particular, in Ref. 21, the authors propose that a well-mixed plantation with two plant types could be an efficient strategy to prevent the dissemination of *Phytophthora* zoospores for plants with high susceptibility. They discuss the percolation threshold of this strategy as a function of the proportion of sown cells, their susceptibilities, and the percentage of inoculated cells (for values less than 10%). However, the control and management of plantation may not be suitable for all cases since different varieties of plants could need specific nutrients and cares. On the other hand, researchers in agronomy sciences have studied the viability and production yield of plantations with intercropping configurations.^{32–34} One of the advantages of this sowing technique is that some plants can develop a certain degree of beneficial interaction between them. Another benefit of intercropping configurations is that they could reduce the number of affected plants by aphid-borne viruses³⁵ or insects transmitted by the movement of herbivores.³⁶ Intercropping plantations are a worldwide extended practice that helps to increase the total production and the efficiency of the land.³⁷ For instance, China has one of the biggest areas in the world dedicated to intercropping cultivates.³⁸ In Western Europe, wheat-based intercropping systems are explored as an agroecological strategy to improve the quality of the grains.³⁹ In North America, cereal yield has been increased during the last decade using this technique.⁴⁰ Remarkably, “milpa” systems (see

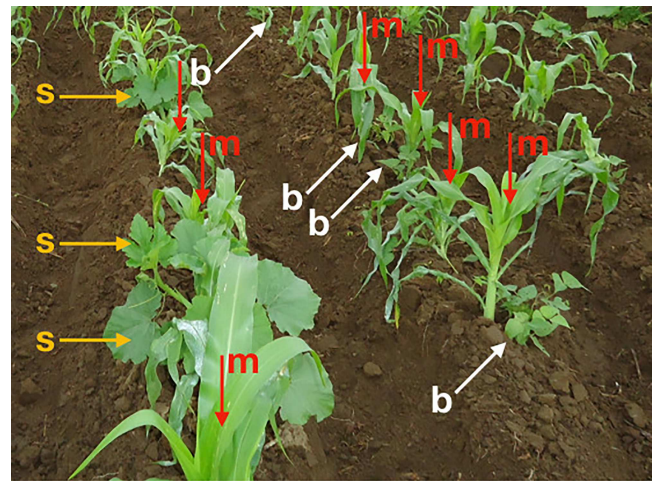


FIG. 1. Example of a traditional Mexican milpa system where maize (m), bean (b), and squash (s) are sown in an intercropping configuration. The importance of this type of plantation lays in the beneficial interaction between species.

Fig. 1) in Mexico represent an ancient agrobiodiverse practice of intercropping plantation.⁴¹ In these polycropping systems, maize, squash, beans, or another legume are seeded in an intercropped configuration.

In this work, we simulate the propagation process of *Phytophthora* over two different planting configurations. In one of them, two types of plants are placed in alternate columns, while in the other, they are placed in alternate diagonals, as depicted in Figs. 2(a) and 2(b), respectively. The spreading process of *Phytophthora* is modeled as a transport phenomenon over a percolating system where the occupied sites represent the plants that may get sick after the interaction with the pathogen. Experimentally, it is observed that not all the plants are affected after the exposure. To account for this, we define the plant’s pathogen susceptibility (χ) as the probability that a plant becomes ill after being exposed to the pathogen. The individuals that exhibit resistance produced an effective immune response (cell wall strengthening, the encoding of enzymes, and synthesis of metabolites against oomycetes and fungal pathogens, among others⁴²). These resistant plants can act as natural barriers that avoid local propagation of the pathogen.^{21,22}

In the rest of this paper, we present the description of the model and the implementation of the simulation method. The percolation threshold is studied for the aforementioned intercropping configurations, and we determine the conditions that prevent the formation of a spanning cluster of susceptible or diseased plants as a function of susceptibilities, occupation density, and the percentage of inoculated cells at the beginning of the propagation process.

II. SIMULATION METHOD AND DATA ANALYSIS

The plantation is modeled as a square lattice of size $L \times L$ in whose cells only one plant can be sown, either type *A* or *B*, with susceptibility χ_A or χ_B , according to an intercropping configuration. The lattice spacing, i.e., the separation between adjacent plants, is

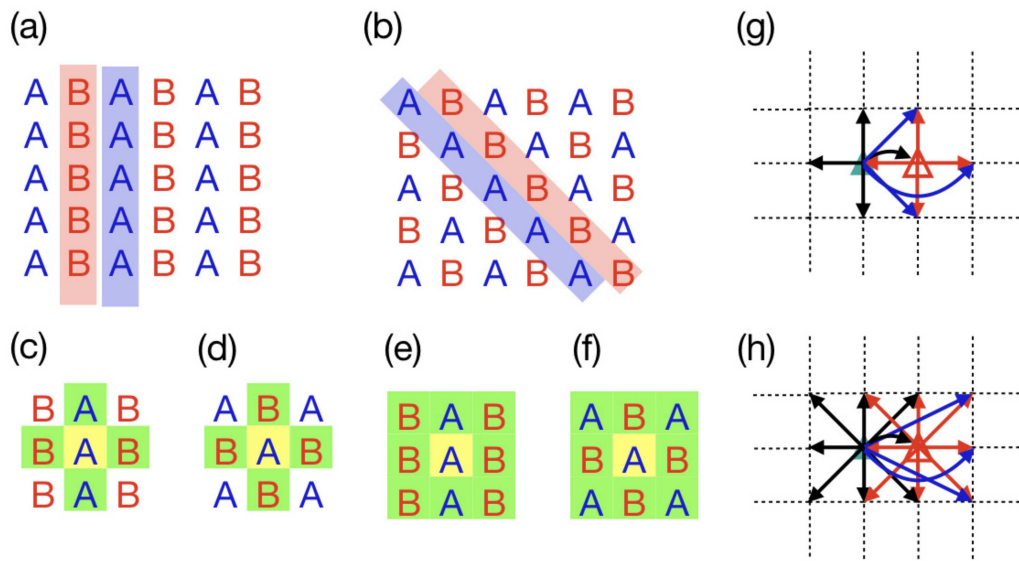


FIG. 2. Intercropping configurations in alternate columns (a) and alternate diagonals (b), with the corresponding local propagation of the pathogen in nearest [(c) and (d)] and next-to-nearest neighbor [(e) and (f)] square lattices. Cells filled in yellow represent a site with a type A plant, and its neighbor cells are marked in green. Subfigures (g) and (h) show the modification to the adjacent neighbor definition induced by inoculated cells (red triangle) that are either empty cells or occupied by a resistant plant but adjacent to a susceptible plant (green triangle) in nearest and next-to-nearest neighbor square lattices, respectively. As a consequence of the micro-organism mobility (red arrows), the nearest-neighbor definition (black arrows) is modified since the site with the susceptible plant can now be linked to farther sites (blue arrows).

chosen as the maximum distance that the pathogen can move before starving or entering in a state of dormancy. This guarantees that the micro-organism can only be spread over the adjacent neighbors. Specifically, we analyze the plantation configurations described in Figs. 2(a) and 2(b) considering nearest and next-to-nearest neighbor square lattices. This allows us to compare the collective behavior of the local propagation for the two models. For example, suppose that the type B plant has a higher resistance than the type A plant; i.e., $\chi_B < \chi_A$. In the nearest-neighbor case, we observe that, in the model with alternate diagonals, a type A plant is completely surrounded by type B plants [see Fig. 2(d)], which can induce a decrease in the rate of the pathogen transmission. In contrast, the model of alternate columns promotes cluster formation through the vertical lines [see Fig. 2(c)]. Besides, for the next-to-nearest neighbor, the alternate column model still promotes the propagation over the columns with plants of higher susceptibility [see Fig. 2(e)], while in the model of alternate diagonals, the pathogen will have a higher probability to propagate over the diagonals [see Fig. 2(f)].

Another important variable in our model is the percentage of cells with the pathogen presence at the beginning of the propagation process, which we will denote by I . This parameter can be interpreted as the probability of observing the pathogen in a cell after a soil test. The propagation process is started at these inoculated cells. We also consider that some cells can be empty with probability $1 - p$. Taking into account all of the above, note that cells in the lattice will have different conditions of occupation and inoculation, which will permit or block the local propagation. Notice that empty cells, or cells with a resistant plant, do not take part in the clustering process, but if they are inoculated at the beginning

of the propagation process and they are adjacent to a susceptible plant, they can act like a *bridge* connecting sites further away than the lattice's spacing. This can be interpreted as a modification of the adjacent neighbor definition. Figures 2(g) and 2(h) show the modified pathogen ranges due to the interaction previously described. All these effects must be taken into account in the simulation.

In our computational implementation, each cell in the plantation is assigned two (independent) states: inoculation and occupancy (by a susceptible plant). These are represented with corresponding Boolean variables. The inoculated cells at the beginning of the propagation process are considered uniformly distributed and independent of its neighbors. Once the value of I has been fixed, a fraction I of cells are randomly chosen to be assigned as inoculated. To do this, the number of inoculated cells (n_I) is randomly generated from the binomial distribution $\mathcal{B}(L^2, I)$. Then, we take n_I elements from the lattice at random and its corresponding inoculation state variable is updated to 1, indicating the presence of the pathogen.

Since the intercropping configuration distinguishes sites that are sowed with type A and B plants, it is possible to form subsets of cells, \mathcal{N}_A and \mathcal{N}_B , for each species such that $\mathcal{N} = \mathcal{N}_A \cup \mathcal{N}_B$ is the set of all cells. The occupancy state is allocated by first placing the type A plants using the Hoshen–Kopelman algorithm⁴³ with occupation probability $p\chi_A$. Then, we place the type B plants by using the Newman–Ziff algorithm^{44,45} (over the \mathcal{N}_B cells), taking into account the occurrence of empty cells has probability $1 - p$. At this point, we stop the simulation and store the critical number n_{Bc} of type B plants that were added before the spanning cluster emerged. For the clustering process, we use the Union-Find algorithm described by Newman and Ziff in Refs. 44 and 45. The rules to connect two

adjacent cells are the following: (i) Both have susceptible plants or (ii) one of the cells is inoculated and the other has a susceptible plant.

Using this algorithm, we compute the relative frequency $f_n^* = f_n/M_T$, where f_n is the number of times the simulation stopped when exactly n type B plants have been added and M_T is the total number of simulation runs. Thus, the probability P_n that a spanning cluster appears in the system after adding n type B plants is determined as

$$P_n = \sum_{k=0}^n f_k^* \quad (1)$$

We estimate the percolation probability after adding the type B plants as

$$P(\chi_B) = \sum_n \mathcal{B}(L^2/2, n, \chi_B) P_n, \quad (2)$$

where

$$\mathcal{B}(L^2/2, n, \chi_B) = \binom{L^2/2}{n} \chi_B^n (1 - \chi_B)^{L^2/2 - n} \quad (3)$$

is the binomial probability mass function. For simplicity, we choose even numbers for L . This means that we have the same number of sites assigned to each type of plants. In Eq. (3), the argument n in \mathcal{B} indicates that there are exactly n sites occupied with a plant in the system (out of $L^2/2$ cells dedicated to the type B plants) when its susceptibility is χ_B . Thus, the critical value χ_B required

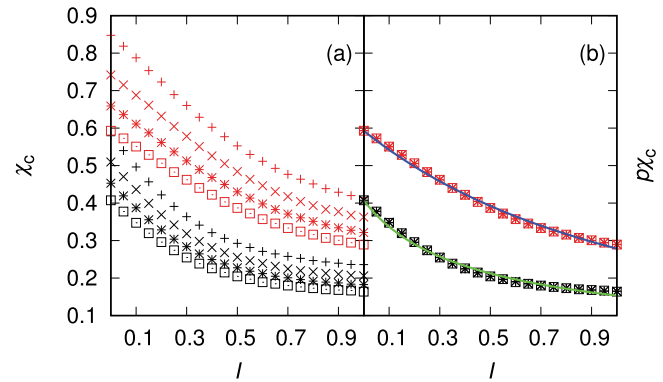


FIG. 4. (a) Percolation thresholds for the case of monoculture plantation as a function of l . The red points, from top to bottom, correspond to $p = 0.7, 0.8, 0.9,$ and 1 for nearest-neighbor square lattices. In the same order, black points for next-to-nearest neighbor square lattices. (b) The collapse of the points $p\chi_c$ for different occupation probabilities ρ . Lines are fits to the data [see Eq. (5)] with $\rho = 1$.

for the emergence of the spanning cluster is determined by solving the equation $P(\chi_B) = 0.5$. To this end, we estimate the percolation probability running 10^4 simulations for several χ_B -values around the value of n at which f_n takes its maximum value. Then, each data-set

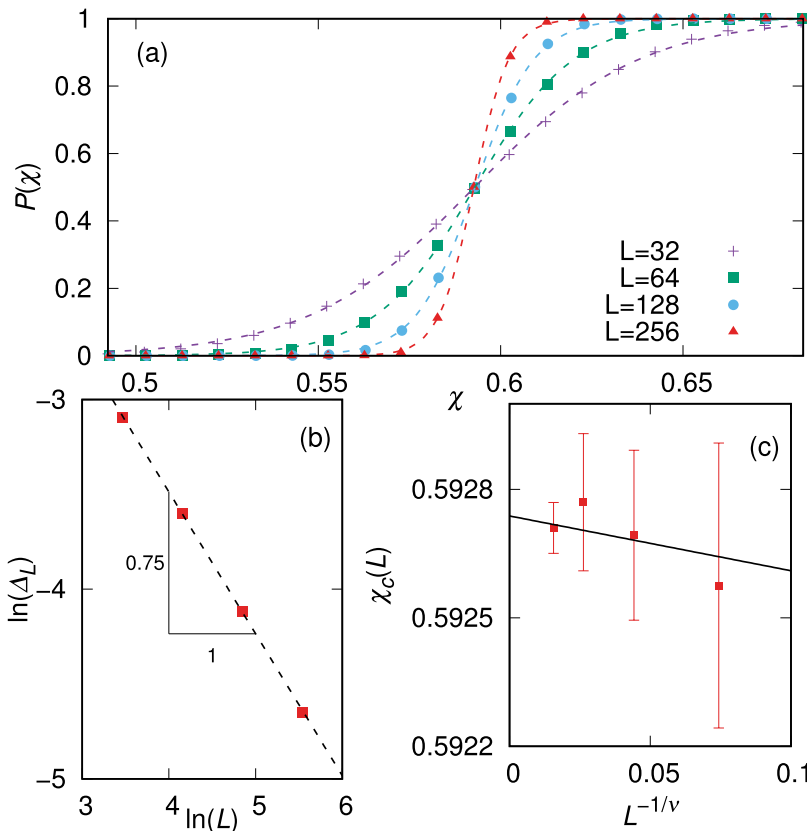


FIG. 3. Determination of the percolation threshold for a nearest-neighbor square lattice with $\chi_A = \chi_B$ and $l = 0$. (a) Percolation probability (figures) as a function of χ for different values of the system size: $L = 32, 64, 128,$ and 256 . Fitting curves [see Eq. (4)] are represented as dashed lines. (b) Δ_L as a function of L in a \ln - \ln scale. The dashed line is the fit $\ln \Delta_L \sim -\nu \ln L$, where the slope is $3/4$. (c) Scaling behavior of $\chi_c(L)$ as a function of $L^{-1/\nu}$ (figures) and the function $\chi_c(L) = mL^{-1/\nu} + \chi_c$ (solid line). In the limit $L \rightarrow \infty$, the intercept corresponds to the percolation threshold in the thermodynamic limit.

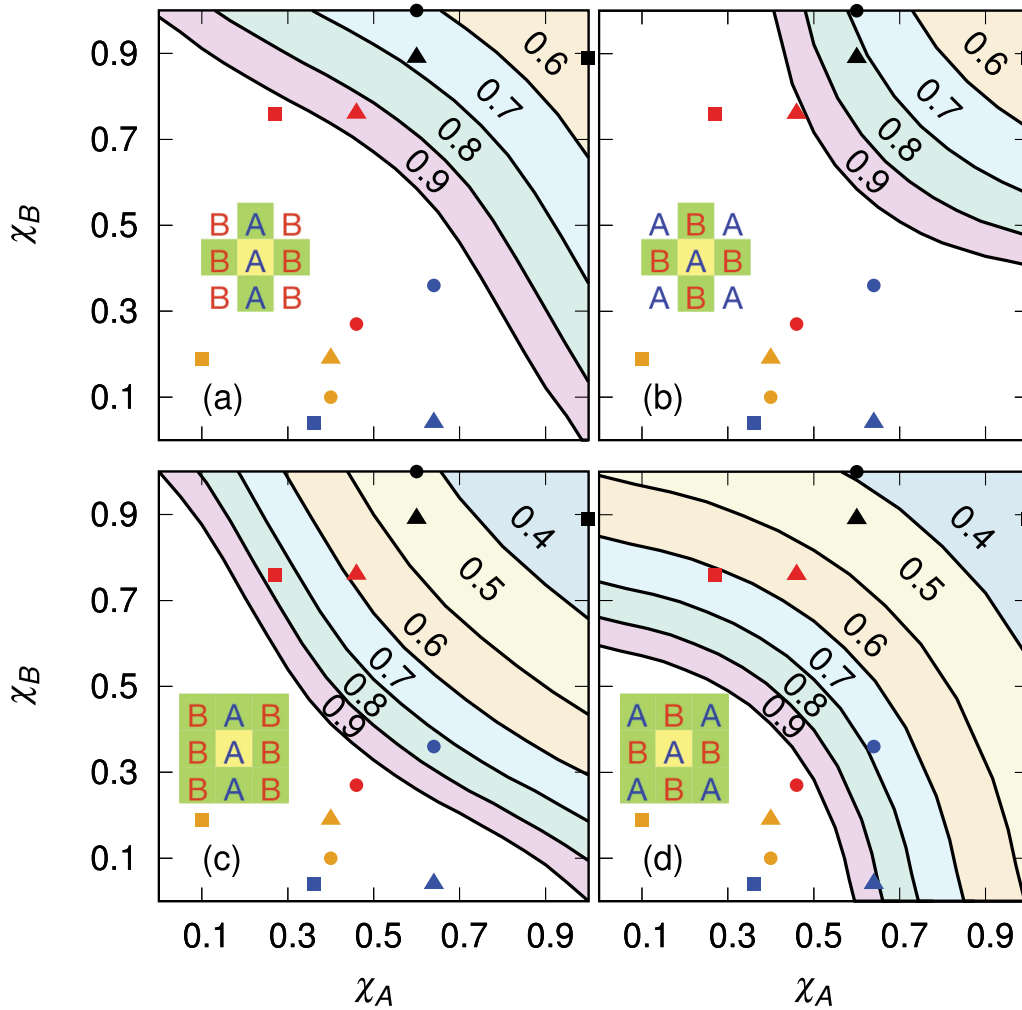


FIG. 5. Phase diagrams for $l = 0$: (a) alternate columns for the nearest neighbor, (b) alternate diagonals for the nearest neighbor, (c) alternate columns for the next-to-nearest neighbor, and (d) alternate diagonals for the next-to-nearest neighbor. The white zone represents the combination of susceptibility values that allow sowing all the cells. Shaded regions indicate the maximum density at which the plantation should be sown to avoid the formation of a spanning cluster. The points represent combinations of different chili susceptibilities: serrano-arbol (circles), serrano-poblano (triangles), and arbol-poblano (squares), exposed to different isolates of *Phytophthora capsici*: PcV01 (black), PcV51 (red), PcV77 (blue), and PcV90 (yellow) (see Table I).

is fitted to the function

$$P(\chi_B) = \frac{1}{2} \left(1 + \tanh \left(\frac{\chi_B - \chi_{Bc}(L)}{\Delta_L} \right) \right), \quad (4)$$

where $\chi_{Bc}(L)$ is the percolation threshold and Δ_L is the width of the sigmoid transition.⁴⁶ To take finite-size effects into account, we also performed simulations using the system size $L = 32, 64, 128,$ and 256 . Thus, the percolation threshold in the thermodynamic limit is estimated by extrapolating the scaling relation $\chi_{Bc} - \chi_{Bc}(L) \propto L^{-1/\nu}$, where ν is the exponent corresponding to the correlation length. It is well known that the transition width Δ_L scales with the system size L as $\Delta_L \propto L^{-1/\nu}$.⁴⁶ From the fit to the percolation probability data, we found that $\nu = 4/3$, which is in good agreement with the results

reported in the literature for the percolation theory in 2D.⁴⁷ In Fig. 3, we show the data analysis to determine the percolation threshold for the case of the nearest-neighbor square lattice with $\chi_A = \chi_B = \chi$ and $l = 0$. Under these conditions, we found the critical susceptibility $\chi_c = 0.59273 \pm 0.00006$, which is in agreement with the best known estimation of the percolation threshold for the classical nearest-neighbor square lattice ($0.59274621 \pm 0.00000013$).⁴⁵

III. RESULTS

The first particular case that we analyze is that in which both types of plants have the same susceptibility ($\chi_A = \chi_B = \chi$). This case does not imply neither that both plants are the same type nor

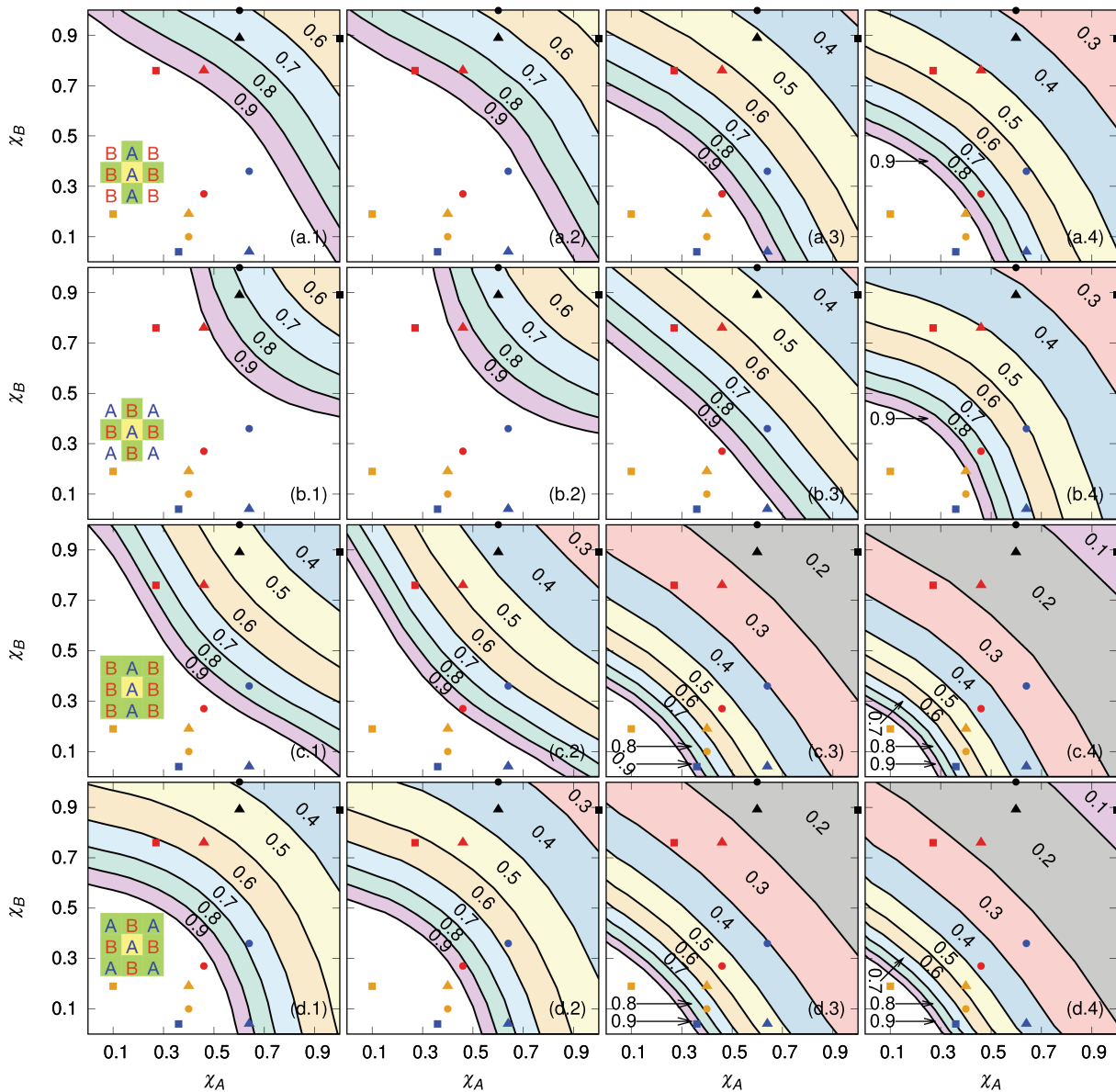


FIG. 6. Phase diagrams for different values of $l = 0.0$ (first column), 0.1 (second column), 0.5 (third column), and 0.8 (fourth column). Rows correspond to alternate columns for the nearest neighbor (first row), alternate diagonals for the nearest neighbor (second row), alternate columns for the next-to-nearest neighbor (third row), and alternate diagonals for the next-to-nearest neighbor (fourth row). Points are the same as in Fig. 5.

that the speed of the propagation front, or the disease, manifests with identical characteristics in both species. However, the clustering of diseased plants at the end of the propagation process would be equivalent to a plantation with only one type of plant.

Figure 4(a) shows the percolation thresholds (χ_c) for the case $\chi_A = \chi_B$. They can be fitted with a q -exponential function⁴⁸

$$\chi_c(I, p) = \frac{p_c}{p(1 + aI/q)^q}, \quad (5)$$

where p_c is the usual critical probability in site percolation, $a = 0.91 \pm 0.03$ and 2.1 ± 0.1 , $q = 2.0 \pm 0.4$ and 0.68 ± 0.06 , for nearest and next-to-nearest neighbor square lattices, respectively. The value of parameter q is in good agreement with the reported values for triangular and *honeycomb* lattices.²² In Fig. 4(b), we show the collapse of the percolation thresholds by plotting $p\chi_c$ as a function of I , where we can see that all of them fit relatively well to the q -exponential function in Eq. (5). This can be understood as the collective contribution of the interaction of susceptible plants

with infected-resistant plants or with inoculated empty cells. Note that the probability of observing this pair becomes higher as χ or p decreases, and I increases. Thus, the percolating system looks like a lattice formed by regular sites and sites involving complex nearest neighbors.²²

One of the most important results for this case is the existence of a percolation threshold that prevents the formation of a spanning cluster of diseased plants even if all the cells have the presence of the pathogen at the beginning of the propagation process. Such values are $0.288\,83 \pm 0.000\,07$ and $0.164\,341 \pm 0.000\,05$ for nearest and next-to-nearest neighbor square lattices, respectively. These values are in good agreement with percolation threshold curves for the square lattices with complex neighborhoods.^{49,50}

On the other hand, the percolation threshold curves for the general case $\chi_A \neq \chi_B$ must satisfy the following properties:

1. The curves have to be decreasing since as one susceptibility increases, the other is expected to decrease.
2. If $\chi_A = \chi_B$, the results obtained must reproduce the case of a single species (see Fig. 4).
3. The percolation threshold must be invariant to the exchange A by B .

Figures 5 and 6 show the phase diagrams obtained using the algorithm proposed for nearest and next-to-nearest neighbor square lattices, with $I = 0.0, 0.1, 0.5$, and 0.8 . Here, the case $I = 0.0$ corresponds to the situation when only one cell in the plantation is inoculated. To exemplify the applications of these results, we plot into the diagrams the combinations of pairs of susceptibilities (χ_A, χ_B) of three different chili varieties exposed to several strains of *P. capsici* (see Table I) reported in Ref. 21. Notice the white zone where sowing is allowed in 100% of the cells. Those are the combinations χ_A and χ_B that assure the disease will not disseminate all over the plantation. Moreover, the shaded zones indicate the maximum occupation probability, for each susceptibility combination, that guarantees the non-emergence of the spanning cluster. The interpretation of these phase diagrams allows us to choose the most adequate sowing configuration and plantation density.

In Fig. 5, we show the phase diagram corresponding to the limit case $I = 0.0$. It is observed that there are substantial differences in the regions that allow sowing the entire plantation among the different models. This phenomenon arises as a collective effect due to differences in the local dissemination of the pathogen in the different sowing configurations [see Figs. 2(c)–2(f)]. Notwithstanding the above, for the same nearest-neighbor definition, this effect is lost as I

increases and the diagrams become similar, as can be noted in Fig. 6 for $I = 0.8$, where the change in the shape of the white zones for both intercropping configurations is almost inappreciable. This is possible since an increase on I rises the numbers of pairs acting as bridges and the clustering of type A with type B plants is highly promoted so that the system undergoes a process of homogenization. Consequently, the barrier effect of resistant plants is lost. This is an indication that there exists a critical value of I for which the use of one or the other intercropping configuration becomes irrelevant.

IV. DISCUSSION AND CONCLUSIONS

In this work, we have presented the analysis of the percolation threshold for the propagation process of *Phytophthora* in two intercropping configurations, alternating columns or diagonals, over nearest and next-to-nearest neighbor square lattices. The relevance of the determination of this critical value is because, at these conditions, the probability that the initial infection point be adjacent or belong to the spanning cluster becomes greater than zero, rising as the susceptibilities or the planting density increases. Then the outbreak could take place on a large part of the plantation.

The most important results are the phase diagrams in Fig. 6, which can help choose the most convenient intercropping configuration and sowing density for a pair of plant types. We found that for a low fraction of inoculated cells at the beginning of the propagation process, for nearest neighbor square lattices, the best option is alternate diagonal plantations since this configuration admits more combinations of susceptibilities that allow planting at 100% of the cells. While in the case of next-to-nearest neighbor square lattices, the best choice is to use the configuration with alternate columns. On the other hand, when I is large, the disease spreading process is indistinguishable for both intercropping configurations. This means that there exists a critical value for I at which the transition between the situations described occurs. This effect was observed when $I \geq 0.5$ for both definitions of adjacent neighbors; nevertheless, a detailed analysis is necessary for a precise determination of this threshold.

Considering *Phytophthora* can survive like saprophytes in adverse environmental conditions, the disease dissemination over the spanning cluster may increase the number of cells with pathogen presence for future cropping cycles. In this case, the yield could be drastically affected even if plants with higher susceptibility values are sown in the next farming.

To show the potential use of the diagrams, we included the combinations of susceptibilities for three chili varieties: “chile de arbol,” “chile poblano,” and “chile serrano” (points in Figs. 5 and 6), which are of high commercial value in Mexico. Notice, in particular, the combination serrano-poblano exposed to the strain PcV77 (blue triangle), with $I = 0.1$, and the next-to-nearest neighbor [see Figs. 6(c.2) and 6(d.2)]. In this case, the configuration of alternate columns allows sowing all the cells in the plantation, while with alternate diagonals, it is required to leave 20% of empty cells to prevent the formation of a spanning cluster, which supposes a decrease in the net yield of the plantation. Another example for the same combination for a different strain (PcV51, red triangles) and $I = 0$, over the nearest neighbor [see Figs. 6(a.1) and 6(b.1)], shows that the entire plantation can be sown if the alternate diagonals are used.

TABLE I. Experimental results of the pathogen susceptibilities for different *Capsicum* varieties: “chile serrano” (χ_s), “chile de arbol” (χ_a), and “chile poblano” (χ_p), exposed to several *Phytophthora* isolates.²¹

Oomycete	χ_s	χ_a	χ_p
PcV01	0.60	1.0	0.89
PcV51	0.46	0.27	0.76
PcV77	0.64	0.36	0.04
PcV90	0.40	0.10	0.19
Blanck test	0	0	0

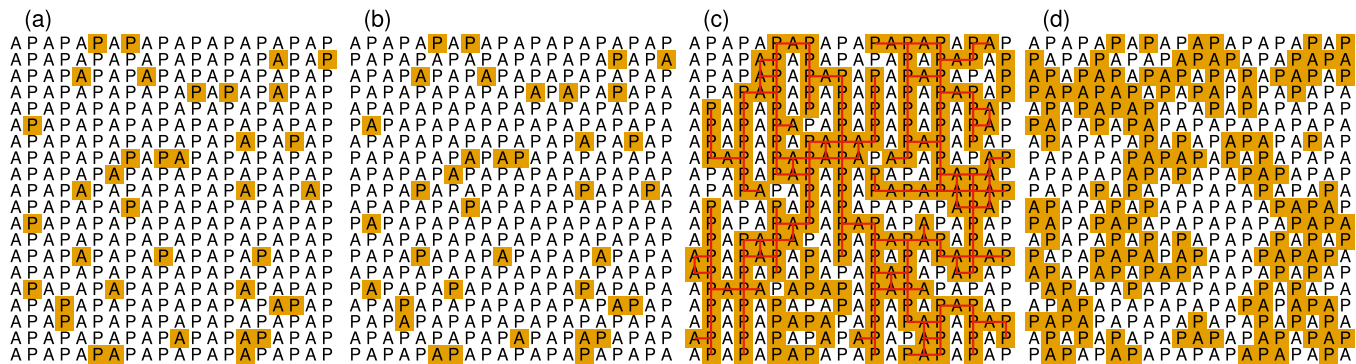


FIG. 7. Examples of the propagation of *Phytophthora* on a nearest-neighbor square lattice for two intercropping configurations, alternating columns [(a) and (c)] and diagonals [(b) and (d)]. The portion of inoculated cells at the beginning of the propagation process is $l = 0.1$, and these cells are shaded in yellow in (a) and (b). The plant type selected are “arbol” (A) and “poblano” (P) chili varieties exposed to the *Phytophthora* strain PcV51 (see Table I for the susceptibility values). In (c) and (d), we show the final state of the dissemination process. Shaded cells indicate plants affected by the pathogen. In (c), the particular combination of values selected for planting density, susceptibilities, and the initial portion of inoculated cells promotes the formation of the spanning cluster (cells connected by red lines).

In Fig. 7, we show an example of *Phytophthora* dissemination under these conditions. Note that in a plantation with alternate columns, the spanning cluster has emerged at the end of the propagation process. On the other hand, a 10% of empty cells would be required in an alternate column plantation.

Finally, planting with an intercropping approach taking into account the conclusions we extracted from the phase diagrams is an effective alternative to avoid the spreading of *Phytophthora* when the spatial homogenization of two (or more) plant types is not suitable. On the other hand, a limitation of our proposal is that we have not taken into account other epidemiological variables. For example, we have experimentally observed the recuperation and reinfection of some individuals. Another feature that we have not yet added to our model is the variability of the maximum distance the pathogen can travel. This distance distribution should be experimentally determined for each pathogen strain, the particular plant variety of interest, and other environmental variables such as soil porosity or humidity. This model also can be extended to analyze more complex intercropping configurations or to consider a higher number of plant varieties. Moreover, some other variables might also be included, such as the care provided by farmers or the possibility of having more than one type of pathogen in the field.

AUTHORS' CONTRIBUTIONS

All authors contributed equally to the designed methodology, data analysis, discussion, and writing of the manuscript and gave final approval for publication.

ACKNOWLEDGMENTS

J.E.R. acknowledges financial support from the CONACyT (postdoctoral fellowship Grant No. 289198). We are grateful to C. Pajares, E. Molina-Gayosso, and J. Lozada-Lechuga for fruitful discussions.

DATA AVAILABILITY






The data that support the findings of this study are available from the corresponding author upon reasonable request.

REFERENCES

- 1A. A. Saberi, “Recent advances in percolation theory and its applications,” *Phys. Rep.* **578**, 1–32 (2015).
- 2R. M. D’Souza, J. Gómez-Gardeñes, J. Nagler, and A. Arenas, “Explosive phenomena in complex networks,” *Adv. Phys.* **68**, 123–223 (2019).
- 3P. E. Seiden and L. S. Schulman, “Percolation model of galactic structure,” *Adv. Phys.* **39**, 1–54 (1990).
- 4M. Braun, J. Dias de Deus, A. Hirsch, C. Pajares, R. Scharenberg, and B. Srivastava, “De-confinement and clustering of color sources in nuclear collisions,” *Phys. Rep.* **599**, 1–50 (2015).
- 5I. Bautista, C. Pajares, and J. E. Ramírez, “String percolation in AA and p+p collisions,” *Rev. Mex. Fis.* **65**, 197–223 (2019).
- 6S. R. Broadbent and J. M. Hammersley, “Percolation processes: I. Crystals and mazes,” *Math. Proc. Cambridge Philos. Soc.* **53**, 629–641 (1957).
- 7D. Stauffer and A. Aharony, *Introduction to Percolation Theory* (Taylor & Francis, 2014).
- 8H. L. Frisch and J. M. Hammersley, “Percolation processes and related topics,” *J. Soc. Ind. Appl. Math.* **11**, 894–918 (1963).
- 9P. Grassberger, “On the critical behavior of the general epidemic process and dynamical percolation,” *Math. Biosci.* **63**, 157–172 (1983).
- 10L. Sander, C. Warren, I. Sokolov, C. Simon, and J. Koopman, “Percolation on heterogeneous networks as a model for epidemics,” *Math. Biosci.* **180**, 293–305 (2002).
- 11J. C. Miller, “Percolation and epidemics in random clustered networks,” *Phys. Rev. E* **80**, 020901 (2009).
- 12D. S. Callaway, M. E. J. Newman, S. H. Strogatz, and D. J. Watts, “Network robustness and fragility: Percolation on random graphs,” *Phys. Rev. Lett.* **85**, 5468–5471 (2000).
- 13M. E. J. Newman, “Spread of epidemic disease on networks,” *Phys. Rev. E* **66**, 016128 (2002).
- 14N. Madar, T. Kalisky, R. Cohen, D. ben Avraham, and S. Havlin, “Immunization and epidemic dynamics in complex networks,” *Eur. Phys. J. B* **38**, 269–276 (2004).
- 15M. W. Shaw, “Modeling stochastic processes in plant pathology,” *Annu. Rev. Phytopathol.* **32**, 523–544 (1994), pMID: 19877847.
- 16D. J. Bailey, W. Otten, and C. A. Gilligan, “Saprotrophic invasion by the soil-borne fungal plant pathogen *Rhizoctonia solani* and percolation thresholds,” *New Phytol.* **146**, 535–544 (2000).

- ¹⁷B. Dybiec, A. Kleczkowski, and C. A. Gilligan, "Controlling disease spread on networks with incomplete knowledge," *Phys. Rev. E* **70**, 066145 (2004).
- ¹⁸G. J. Gibson, W. Otten, J. A. N. Filipe, A. Cook, G. Marion, and C. A. Gilligan, "Bayesian estimation for percolation models of disease spread in plant populations," *Stat. Comput.* **16**, 391–402 (2006).
- ¹⁹W. Otten and C. A. Gilligan, "Soil structure and soil-borne diseases: Using epidemiological concepts to scale from fungal spread to plant epidemics," *Eur. J. Soil Sci.* **57**, 26–37 (2006).
- ²⁰C. C. Mundt and K. E. Sackett, "Spatial scaling relationships for spread of disease caused by a wind-dispersed plant pathogen," *Ecosphere* **3**, 24 (2012).
- ²¹J. E. Ramírez, E. Molina-Gayosso, J. Lozada-Lechuga, L. M. Flores-Rojas, M. I. Martínez, and A. Fernández Téllez, "Percolation strategy to improve the production of plants with high pathogen susceptibility," *Phys. Rev. E* **98**, 062409 (2018).
- ²²J. E. Ramírez, C. Pajares, M. I. Martínez, R. Rodríguez Fernández, E. Molina-Gayosso, J. Lozada-Lechuga, and A. Fernández Téllez, "Site-bond percolation solution to preventing the propagation of *Phytophthora* zoospores on plantations," *Phys. Rev. E* **101**, 032301 (2020).
- ²³D. C. Erwin and O. K. Ribeiro, *Phytophthora Diseases Worldwide* [American Phytopathological Society (APS Press), St. Paul, MN, 1996].
- ²⁴T. Reglinski, M. Spiers, J. Taylor, and M. Dick, "Root rot in radiata pine seedlings can be controlled," *N. Z. J. For. Sci.* **54**, 16–18 (2010), available at http://nzjf.org.nz/abstract.php?volume_issue=j54_4&first_page=16.
- ²⁵T. Jung, A. M. Vettraino, T. Cech, and A. Vannini, "The impact of invasive *Phytophthora* species on European forests," in *Phytophthora: A Global Perspective*, edited by K. Lamour (CABI, London, 2013), Chap. 16, pp. 146–158.
- ²⁶A. R. Hardham and L. M. Blackman, "Phytophthora cinnamomi," *Mol. Plant Pathol.* **19**, 260–285 (2018).
- ²⁷E. Bernhardt and R. Grogan, "Effect of soil matric potential on the formation and indirect germination of sporangia of *Phytophthora parasitica*, *Phytophthora capsici*, and *Phytophthora capsici cryptogea* rots of tomatoes, *Lycopersicon esculentum*," *Phytopathology* **72**, 507–511 (1982).
- ²⁸A. R. Hardham, "Phytophthora cinnamomi," *Mol. Plant Pathol.* **6**, 589–604 (2005).
- ²⁹Y. Cohen and M. D. Coffey, "Systemic fungicides and the control of oomycetes," *Annu. Rev. Phytopathol.* **24**, 311–338 (1986).
- ³⁰A. Drenth and D. I. Gest, "Phytophthora in the tropics," in *Diversity and Management of Phytophthora in Southeast Asia*, edited by A. Drenth and D. I. Gest (ACIAR, 2004), Vol. 114, Chap. Biology of *Phytophthora*, pp. 30–41.
- ³¹Y.-J. Zhang, Z.-X. Wu, P. Holme, and K.-C. Yang, "Advantage of being multi-component and spatial: Multipartite viruses colonize structured populations with lower thresholds," *Phys. Rev. Lett.* **123**, 138101 (2019).
- ³²Y. Hong, N. Heerink, S. Jin, P. Berentsen, L. Zhang, and W. van der Werf, "Intercropping and agroforestry in China—Current state and trends" *Agr. Ecosyst. Environ.* **244**, 52–61 (2017).
- ³³M.-O. Martin-Guay, A. Paquette, J. Dupras, and D. Rivest, "The new green revolution: Sustainable intensification of agriculture by intercropping," *Sci. Total Environ.* **615**, 767–772 (2018).
- ³⁴A. Elhakeem, W. van der Werf, J. Ajal, D. Lucà, S. Claus, R. A. Vico, and L. Bastiaans, "Cover crop mixtures result in a positive net biodiversity effect irrespective of seeding configuration," *Agr. Ecosyst. Environ.* **285**, 106627 (2019).
- ³⁵A. Allen-Perkins and E. Estrada, "Mathematical modelling for sustainable aphid control in agriculture via intercropping," *Proc. R. Soc. A* **475**, 20190136 (2019).
- ³⁶J. E. Banks and B. Ekbom, "Modelling herbivore movement and colonization: Pest management potential of intercropping and trap cropping," *Agric. For. Entomol.* **1**, 165–170 (1999).
- ³⁷Z. Xu, C. Li, C. Zhang, Y. Yu, W. van der Werf, and F. Zhang, "Intercropping maize and soybean increases efficiency of land and fertilizer nitrogen use; A meta-analysis," *Field Crop. Res.* **246**, 107661 (2020).
- ³⁸H. Knörzer, S. Graeff-Hönninger, B. Guo, P. Wang, and W. Claupein, "The rediscovery of intercropping in China: A traditional cropping system for future Chinese agriculture—A review," in *Climate Change, Intercropping, Pest Control and Beneficial Microorganisms*, edited by E. Lichtfouse (Springer, 2004), Vol. 2, pp. 13–44.
- ³⁹M. Gooding, E. Kasyanova, R. Ruske, H. Hauggaard-Nielse, E. Jensen, C. Dahlmann, P. von Fragstein, A. Dibet, G. Corre-Hellou, Y. Crozat, A. Pristeri, M. Romeo, M. Monti, and M. Launay, "Intercropping with pulses to concentrate nitrogen and sulphur in wheat," *J. Agr. Sci.* **145**, 469–479 (2007).
- ⁴⁰D. Tilman, "Benefits of intensive agricultural intercropping," *Nat. Plants* **6**, 604 (2020).
- ⁴¹A. Bermeo, S. Couturier, and M. Galeana Pizaña, "Conservation of traditional smallholder cultivation systems in indigenous territories: Mapping land availability for milpa cultivation in the Huasteca Poblana, Mexico," *Appl. Geogr.* **53**, 299–310 (2014).
- ⁴²S. Serrazina, C. Santos, H. Machado, C. Pesquita, R. Vicentini, M. S. Pais, M. Sebastiana, and R. Costa, "Castanea root transcriptome in response to *Phytophthora cinnamomi* challenge," *Tree Genet. Genomes* **11**, 6 (2015).
- ⁴³J. Hoshen and R. Kopelman, "Percolation and cluster distribution. I. Cluster multiple labeling technique and critical concentration algorithm," *Phys. Rev. B* **14**, 3438–3445 (1976).
- ⁴⁴M. E. J. Newman and R. M. Ziff, "Efficient Monte Carlo algorithm and high-precision results for percolation," *Phys. Rev. Lett.* **85**, 4104–4107 (2000).
- ⁴⁵M. E. J. Newman and R. M. Ziff, "Fast Monte Carlo algorithm for site or bond percolation," *Phys. Rev. E* **64**, 016706 (2001).
- ⁴⁶M. D. Rintoul and S. Torquato, "Precise determination of the critical threshold and exponents in a three-dimensional continuum percolation model," *J. Phys. A: Math. Gen.* **30**, L585–L592 (1997).
- ⁴⁷A. Coniglio, "Cluster structure near the percolation threshold," *J. Phys. A: Math. Gen.* **15**, 3829–3844 (1982).
- ⁴⁸T. Yamano, "Some properties of q-logarithm and q-exponential functions in Tsallis statistics," *Physica A* **305**, 486–496 (2002).
- ⁴⁹K. Malarz and S. Galam, "Square-lattice site percolation at increasing ranges of neighbor bonds," *Phys. Rev. E* **71**, 016125 (2005).
- ⁵⁰M. Majewski and K. Malarz, "Square lattice site percolation thresholds for complex neighbourhoods," *Acta Phys. Pol. B* **38**, 2191 (2007), available at <https://www.actaphys.uj.edu.pl/R/38/6/2191/pdf>.

Site percolation threshold of composite square lattices and its agroecology applications

D. Rosales Herrera ¹, Jorge Velázquez-Castro ^{1,*}, A. Fernández Téllez ¹, Jesús F. López-Olguín ^{2,3} and J. E. Ramírez ^{3,†}

¹*Facultad de Ciencias Físico Matemáticas, Benemérita Universidad Autónoma de Puebla, Apartado Postal 165, 72000 Puebla, Pue., Mexico*

²*Herbario y Jardín Botánico, Vicerrectoría de Investigación y Estudios de Posgrado, Benemérita Universidad Autónoma de Puebla, Apartado Postal 165, 72000 Puebla, Pue., Mexico*

³*Centro de Agroecología, Instituto de Ciencias, Benemérita Universidad Autónoma de Puebla, Apartado Postal 165, 72000 Puebla, Pue., Mexico*



(Received 29 August 2023; accepted 1 December 2023; published 11 January 2024)

We analyze the percolation threshold of square lattices comprising a combination of sites with regular and extended neighborhoods. We found that the percolation threshold of these composed systems smoothly decreases with the fraction of sites with extended neighbors. This behavior can be well-fitted by a Tsallis q -Exponential function. We found a relation between the fitting parameters and the differences in the gyration radius among neighborhoods. We also compared the percolation threshold with the critical susceptibility of nearest and next-to-nearest neighbor monoculture plantations vulnerable to the spread of phytopathogen. Notably, the critical susceptibility in monoculture plantations can be described as a linear combination of two composite systems. These results allow the refinement of mathematical models of phytopathogen propagation in agroecology. In turn, this improvement facilitates the implementation of more efficient computational simulations of agricultural epidemiology that are instrumental in testing and formulating control strategies.

DOI: [10.1103/PhysRevE.109.014304](https://doi.org/10.1103/PhysRevE.109.014304)

I. INTRODUCTION

Percolation theory is usually associated with the study of transport phenomena occurring through porous media [1–3]. This theory arises from the observations made by Broadbent when he was designing charcoal filters for gas masks and measuring their efficiency. Later, in collaboration with Hammersley, Broadbent concluded that transporting a fluid (or individual particles) through a random media with a certain fraction of open (or closed) bonds defines a new kind of diffusion process [4]. Between 1954 and 1957, the percolation theory was formalized and thenceforth studied as a mathematical framework based on geometry and probability [4–6]. In this theory, the simplest way of modeling a porous media is by means of a square lattice, wherein each cell is assigned to be occupied with probability p or empty with the complementary probability $1 - p$ [3,7]. This assignment is carried out independently of the occupation state of the neighbor cells. By construction, the transport phenomena can only occur across the occupied cells. Notice that for small p values, there are few occupied cells in the system, and then the transport phenomenon cannot take place. On the other hand, if p takes values close to 1, the occupied cells fill the system, mostly grouped in a single giant cluster, named the spanning cluster, that connects the system from one side to the opposite side. The emergence of the spanning cluster in the system guarantees that the transport phenomenon occurs.

The fundamental problem to solve in percolation theory is determining the minimal probability value required for the emergence of the spanning cluster. This critical value is known as the *percolation threshold*, which should be estimated for each specific problem [8].

Percolation theory has a wide diversity of applications, ranging from the study of the formation of galactic structures to the description of the formation and properties of the quark-gluon plasma [8–11]. Moreover, the analysis of the connection properties of the graph defined by social interactions and the main epidemiological parameters of diseases shed light on the development of mobility public policies that avoid the spacial propagation of epidemics [12,13].

Recently, in Refs. [14–17], the authors proposed a novel application of percolation theory in agronomy as an agroecological strategy to prevent the dissemination of harmful phytopathogens on plantations. In particular, they analyze the propagation of *Phytophthora* (from Greek, literally meaning plant destroyer) zoospores, micro-organisms classified as oomycetes that cause epiphytic interactions with the most destructive effects that attack the root of plants and trees in every corner of the world [18]. These zoospores swim chemotactically toward the plants using flagella, which can disperse through water films or soil moisture, including those on the surface of plants [18,19]. Many species of *Phytophthora* can persist as saprophytes if the environmental conditions are not appropriate but become parasitic in the presence of susceptible hosts [20,21]. Damages produced by this phytopathogen primarily concentrate in the root of plants but also include rotting in seedlings, tubers, corms, the base of the stem, and other organs. The diseases caused by exposure to

*jorgevc@fcfm.buap.mx

†jhony.ramirezcanino@viep.com.mx

Phytophthora generate tremendous losses in agronomy and forestry. Due to the physiology of the oomycetes, most fungicides or antibiotics have no effects on them, motivating the research on nonchemical strategies that minimize or mitigate the propagation of the pathogen [18,22,23].

On the other hand, in laboratory experiments or *in situ* observation, it has been noted that some plants manifest the disease after the exposition to the pathogen, while others do not get sick because some individuals can deploy defense mechanisms against the infestation process (resistant plants) [14,15]. There are no methods to distinguish what seed will grow as a resistant plant. This fact allows us to define the plant susceptibility χ as the probability of an individual getting ill after the interaction with the phytopathogen, which can be experimentally measured through the determination of the survival rate of exposed plants.

In the context of percolation theory, the problem of *Phytophthora* propagation on a plantation can be modeled as a transport phenomenon on a regular lattice [14,16]. These systems are proposed to be studied on square lattices for simplicity. In a first approach, the lattice spacing can be chosen as the maximal length distance that zoospores can travel before starving or entering a state of dormancy. This guarantees that the micro-organisms can be spread over the adjacent plants. Under these considerations, this problem is directly mapped to a propagation process occurring on a square lattice with nearest neighbors, wherein occupied sites correspond to susceptible plants.

Another relevant ingredient of this model is the fraction of cells with the pathogen presence at the beginning of the propagation process. These cells are assumed to be uniformly and randomly distributed on the plantation. The propagation process is started in these inoculated cells. By construction, the zoospores move only at the adjacent cells, and they reproduce if they reach a susceptible plant. On the contrary, the zoospores die or enter into a dormancy state if they arrive at a resistant plant or an empty cell. However, the inoculated cells at the beginning of the propagation process have a fascinating behavior if they are adjacent to a susceptible plant and simultaneously occupy empty cells or cells with resistant plants. Under this condition, the inoculated cells act as bridges, connecting plants beyond the neighborhood definition, as we depict in Fig. 1 for square lattices with nearest and next-to-nearest neighbors. Moreover, the authors of Refs. [15,16] suggest that the systems look like a square lattice with regular sites together with a fraction of sites with an extended neighborhood in the lattice.

In this work, we introduce the model of site percolation with a combination of two different nearest neighbor definitions, one with a neighborhood more extended than the other. These sites with extended neighborhoods play a similar role to the inoculated cells under the conditions described above. In the same way as in the percolation-agroecological model, the number of extended sites is controlled by the probability I . We compute the percolation threshold through computer simulations for a wide range of neighborhood combinations and I ranging from 0 to 1.

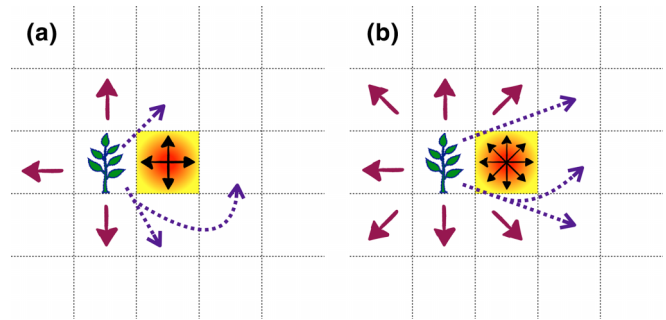


FIG. 1. Sketch of the interaction of an inoculated empty cell adjacent to a susceptible plant on (a) 2N and (b) 3N plantations. Despite *Phytophthora* zoospores moving accordingly to the neighbor definition (solid arrows), they can connect susceptible plants beyond the vicinity (dotted arrows), forming bridges that promote the formation of the spanning cluster.

The plan of the paper is as follows. In Sec. II, we provide the simulation and data analysis methods. In Sec. III, we show our results of the percolation threshold for the systems of interest. In Sec. IV, we discuss the applications of composite systems to model the propagation of phytopathogens on plantations. Finally, Sec. V contains the discussion of our results, conclusions, and perspectives.

II. SIMULATION METHOD AND DATA ANALYSIS

We use the Newman-Ziff simulation scheme [24,25] to determine the site percolation threshold of composite square lattices. This algorithm consists of measuring a particular observable O_n after adding exactly n sites. Therefore, the average $\langle O \rangle$ is computed at a particular p value by convoluting the O_n determinations with the fluctuations of the occupation probability. In Fig. 2 we show the neighborhood definitions used in this work: (a) nearest neighbors (2N), (b) next-to-nearest neighbors (3N). For the sake of notation, we denote as Ext1, Ext2, and Ext3 the extended neighborhoods in Figs. 2(c), 2(d) and 2(e), respectively. We explore the percolation threshold of square lattices considering all the possible pair combinations of these nearest neighbor definitions. In what follows, for a given pair combination, we call extended sites those with the larger neighborhood; meanwhile, the sites with the smaller ones are named regular sites.

In the simulation, we randomly add site by site. Each added site is randomly chosen to be regular or extended with probabilities $1 - I$ and I , respectively. Since in the lattice there are sites with two kinds of neighborhood definitions, we must pay special attention to the clustering process, which is performed by using the Union-Find algorithm. To do this, we assign different labels to sites in the system. However, if two sites belong to the same cluster, we update their labels to have the same value. For each site added, we first check the occupation states of every cell in the regular vicinity, and the site is merged with the cluster to which the occupied neighbor sites belong. Then, the complementary extended neighborhood is checked, but the clustering process fulfills the following rules: (i) if the added site is regular, it is only merged with the occupied extended sites; (ii) otherwise, the added extended

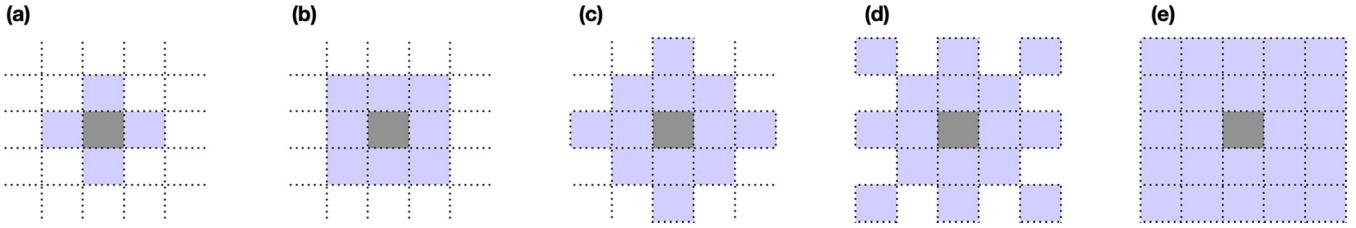


FIG. 2. Neighborhoods discussed in this manuscript: (a) 2N, (b) 3N, (c) Ext1, (d) Ext2, and (e) Ext3.

site is merged with all the occupied sites. In the simulation process, we consider systems with free boundary conditions.

The simulation is stopped when the spanning cluster emerges in the system. This occurs when, for the first time, sites on opposite sides of the lattice acquire the same label. At this point, we store the number of sites added. Using the information from 10^6 simulations, we construct the probabilities f_n and $F_n = \sum_{k=1}^n f_k$ of observing the emergence of the spanning cluster after adding exactly and at most n sites, respectively.

In the Newman-Ziff simulation scheme for a square lattice with L^2 sites, the average of an observable O at an arbitrary value of the occupation probability is computed as

$$O(p) = \sum_{n=1}^{L^2} O_n B(L^2, n, p), \quad (1)$$

where O_n is the value of the observable when there are exactly n occupied sites in the system, and $B(L^2, n, p)$ is the probability mass function of the binomial distribution, which counts the fluctuations of the number of occupied sites for a system filled with occupation probability p . Therefore, we compute the percolation probability by plugging the distribution F_n in (1), that is,

$$P_L(p) = \sum_{n=1}^{L^2} F_n B(L^2, n, p). \quad (2)$$

In Eq. (2), we have added the subscript L to denote the percolation probability dependence on the system size. To avoid the difficulties that carry the computation of the factorial of large numbers, we compute the binomial weights by using the following recursive formula [25]:

$$B(L^2, n, p) = \begin{cases} B(L^2, n-1, p) \frac{L^2-n+1}{n} \frac{p}{1-p} & \text{if } n > n_m, \\ B(L^2, n+1, p) \frac{n+1}{L^2-n} \frac{1-p}{p} & \text{if } n < n_m, \end{cases}$$

where $n_m = pL^2$ is the n -value where the probability mass function of the binomial distribution takes its maximum value. Moreover, we set $B(L^2, n_m, p) = 1$. In this way, the percolation probability (2) must be normalized by dividing by $\sum_{n=1}^{L^2} B(L^2, n, p)$.

After the computation of the percolation probability, the data set is fitted to the sigmoid function

$$P_L(p) = \frac{1}{2} \left[1 + \tanh \left(\frac{p - p_{cL}}{\Delta_L} \right) \right], \quad (3)$$

where p_{cL} is the estimation of the percolation threshold under the conditions of the systems in the simulation, and Δ_L is the width of the sigmoid transition [26]. To take into account

finite-size effects on the percolation threshold, we perform simulations with different system sizes, $L = 32, 48, 64, 96, 128, 192, 256, 384,$ and 512 . Moreover, for each case under study, we determine the percolation threshold for a wide variety of values of the fraction of extended sites, starting at $I = 0$ until $I = 1$ with increments of $\Delta I = 0.05$. The data analysis is performed with the information of 10^6 simulations for each estimation of p_{cL} . In all cases, the well-known scaling relation $\Delta_L \propto L^{-1/\nu}$ for the width of the sigmoid transition is satisfied with $1/\nu \sim 0.75$, which is the universal value of the exponent corresponding to the correlation length found for 2D percolation systems [27].

Finally, we estimate the percolation threshold in the thermodynamic limit (p_c) by analyzing the scaling relation of $p_c - p_{cL}$ as a function of L . It has been previously observed that the free boundary conditions led to $p_c - p_{cL} \propto L^{-2/\nu}$ [10], which is a stronger finite-size effect than the universal scaling relation for the percolation threshold for finite lattices, given by $p_c - p_{cL} \propto L^{-1/\nu}$ [28]. We observe a good agreement of our data sets with the latter scaling relation. Therefore, we estimate the percolation threshold in the thermodynamic limit ($L \rightarrow \infty$) by extrapolating the trend of p_{cL} as a function of $L^{-2/\nu}$. In Sec. III, we summarize our estimations of the percolation threshold for all the possible combinations of neighborhood pairs depicted in Fig. 2.

III. RESULTS

We recall that there are sites with two different neighborhood definitions in the system. The number of each type of site is controlled by the parameter I . Given the value of I , the probability of adding a regular or extended site is $1 - I$ or I , respectively. Notice that there are two limit cases. When $I = 0$ or 1 , only regular or extended sites are added to the system. These results are summarized in Table I. Our estimations of p_c for square lattices with 2N and 3N neighbors are in agreement with the best estimation of the percolation threshold reported in the literature. Moreover, for the extended neighborhoods

TABLE I. Percolation threshold, coordination number, and gyration radius of the neighborhoods discussed in this manuscript.

Neighborhood	Coordination number	p_c	R_g^2
2N [Fig. 2(a)]	4	0.592741(5)	4/5
3N [Fig. 2(b)]	8	0.40721(1)	4/3
Ext1 [Fig. 2(c)]	12	0.289117(9)	28/13
Ext2 [Fig. 2(d)]	16	0.20900(1)	60/17
Ext3 [Fig. 2(e)]	24	0.16466(2)	4

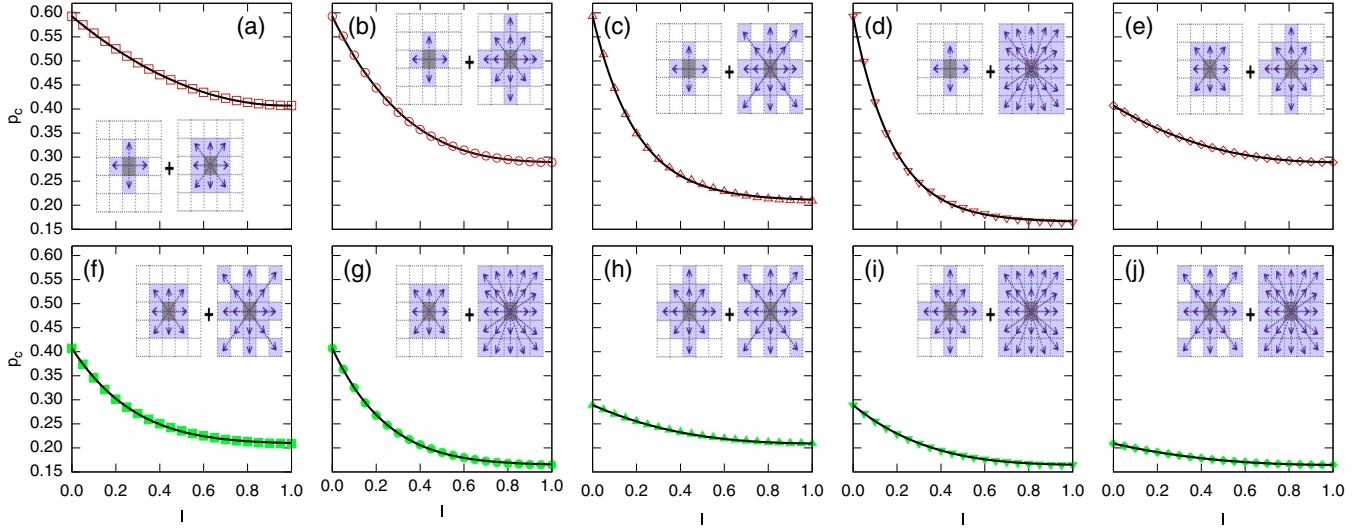


FIG. 3. Percolation threshold of composite square lattices (figures) together with their corresponding fitting function (solid lines). The neighborhood combinations are the following: (a) 2N+3N (empty red squares), (b) 2N+Ext1 (empty red circles), (c) 2N+Ext2 (empty red triangles), (d) 2N+Ext3 (empty red inverted triangles), (e) 3N+Ext1 (empty red diamonds), (f) 3N+Ext2 (filled green squares), (g) 3N+Ext3 (filled green circles), (h) Ext1+Ext2 (filled green triangles), (i) Ext1+Ext3 (filled green inverted triangles), and (j) Ext2+Ext3 (filled green diamonds).

Ext1, Ext2, Ext3, we have improved the previous estimations performed by Malarz in two digits [29,30].

In Fig. 3, we show our estimations of the percolation threshold in the thermodynamic limit for square lattices with a combination of regular and extended sites as a function of I . In all cases, p_c smoothly decreases from $p_{c,\text{reg}}$ to $p_{c,\text{ext}}$ as I increases, where $p_{c,\text{reg}}$ and $p_{c,\text{ext}}$ denote the percolation threshold for square lattices with only regular or extended sites, respectively. Despite the fact that the mean coordination number of the composite system $\bar{z} = z_{\text{reg}} + I(z_{\text{ext}} - z_{\text{reg}})$ has a linear dependence on I , the percolation threshold for these systems does not response linearly nor inversely as a function of I . Notice that, at low values of the fraction of extended sites, the percolation threshold rapidly varies from $p_{c,\text{reg}}$ because of the presence of the extended sites. In fact, p_c decays exponentially for low values of I , as further discussed below. On the contrary, for values of I close to 1, p_c asymptotically reaches the value of $p_{c,\text{ext}}$, which means that the connectivity of the system is primarily due to the extended sites.

Additionally, we found that the percolation threshold of the system with combined neighbor definitions can be well fitted with a Tsallis q -Exponential function

$$p_c = p_{c,\text{ext}} + (p_{c,\text{reg}} - p_{c,\text{ext}}) \left(1 - \frac{I}{\lambda n}\right)^n, \quad (4)$$

where $n = 1/(1 - q)$ defines the q parameter of the Tsallis function. In particular, for the cases 2N+Ext2 and 2N+Ext3, it is found that n takes large values; thus, we replace the Tsallis q -Exponential function for an exponential function. Table II summarizes the value of the fitting parameters for the cases discussed in this paper. The obtained fitting functions are shown as solid lines in Fig. 3. It is worth mentioning that the obtained n -values lead to $q < 1$, so the range of the fitting function is restricted to be $I < \lambda n$ [31], for which in almost all cases it occurs that $\lambda n > 1$, except for the combination

2N+3N. In this case, we obtain $\lambda n \approx 0.98$, and p_c takes complex values for $I > 0.98$. However, the imaginary part of p_c is of the order of 10^{-6} for $0.98 < I \leq 1$, which can be neglected, and the fitting function is extended to the rest of the interval $[0,1]$ by taking the real part of (4).

Note that the series expansion of (4) around $I = 0$ approximates the Tsallis q -Exponential to an exponential decay given by

$$p_c - p_{c,\text{ext}} \propto 1 - \frac{I}{\lambda} + O(I^2) \approx e^{-I/\lambda}, \quad (5)$$

where the factor $1/\lambda$ is the decay constant. In Fig. 4, we show this exponential behavior for all the neighborhood combinations discussed in this manuscript. In some instances, the p_c curve is scaled by a factor of 10^4 to improve visualization. Note the agreement of the estimated percolation threshold for low values of I with the exponential function with a constant decay $1/\lambda$, where λ is taken from Table II.

TABLE II. Fit parameter values obtained for the percolation threshold of all the composite systems discussed in this manuscript.

Neighborhood	λ	n
2N+3N	0.488(7)	2.01(2)
2N+Ext1	0.33(1)	3.8(1)
2N+Ext2	0.201(1)	> 10
2N+Ext3	0.183(1)	> 10
3N+Ext1	0.428(5)	2.54(3)
3N+Ext2	0.28(3)	6.7(5)
3N+Ext3	0.25(3)	9.0(8)
Ext1+Ext2	0.40(1)	2.95(7)
Ext1+Ext3	0.33(1)	4.0(1)
Ext2+Ext3	0.432(5)	2.48(2)

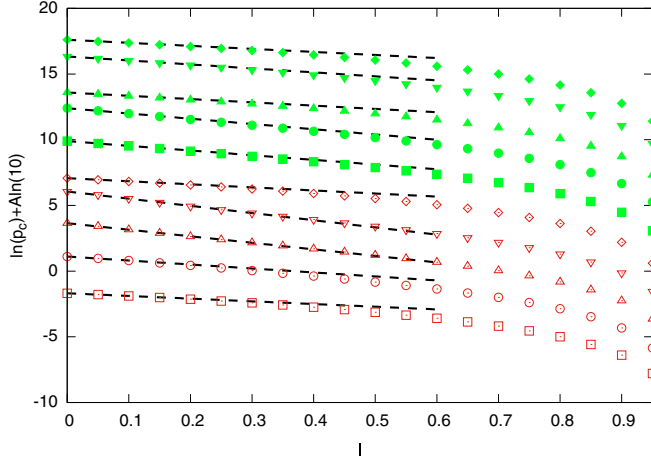


FIG. 4. Exponential behavior of composite systems at low values of I (figures) together with their exponential approximation (dashed lines). Figures and colors are the same as in Fig. 3.

Moreover, we found relationships between the fitting parameters and the difference in the radius of gyration of the extended and regular neighborhoods (see Fig. 5) as follows:

$$\lambda = c_2 e^{-c_1(R_{g,\text{ext}} - R_{g,\text{reg}})}, \quad (6)$$

$$\frac{1}{n} = m(R_{g,\text{ext}} - R_{g,\text{reg}}) + b, \quad (7)$$

with $c_1 = 1.13(3)$, $c_2 = 0.62(2)$, $m = -0.62(4)$, and $b = 0.61(3)$. $R_{g,\text{ext}}$ and $R_{g,\text{reg}}$ are the gyration radius of the extended and regular neighborhoods, respectively. The gyration radius is computed as

$$R_g^2 = \frac{1}{z+1} \sum_k z_k r_k^2, \quad (8)$$

where z_k is the number of possible neighboring sites at a distance r_k from the center of the figure, and z is the coordination number. In Table I, we show the values of R_g^2 for the neighborhood definitions under study. For the cases $2N+\text{Ext}2$

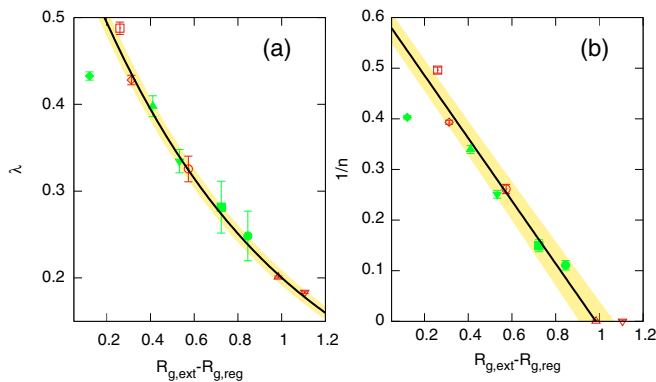


FIG. 5. Trend of the fit parameters (a) λ and (b) $1/n$ as functions of the difference in the neighborhood gyration radius of composite systems (figures). Solid lines correspond to the fitting functions of Eqs. (6) and (7), respectively. Shaded regions are the error propagation of the fitting functions. Figures and colors are the same as in Fig. 3.

and $2N+\text{Ext}3$, we take $1/n \rightarrow 0$. In Sec. IV, we discuss how our results could be useful for understanding and modeling the propagation of phytopathogens on plantations.

IV. APPLICATION TO AGROECOLOGY

The propagation of *Phytophthora* zoospores has been previously studied as a percolation problem in Refs. [14–16]. In these studies, the authors discussed the characteristics needed for the formation of a spanning cluster of diseased and susceptible plants. The latter situation marks the onset of the outbreak on the plantation. It was shown that the percolation threshold depends substantially on the geometry of the plantation and the percentage of inoculated cells at the beginning of the propagation process. Inoculated sites that, at the same time, are empty or occupied with a resistant plant play the role of bridges connecting sites further away from the neighborhood definition.

Let us comment on the computational implementation for a monoculture plantation. The plantation is modeled as a regular lattice where its cells are assigned two independent occupancy states: inoculation and occupation by a susceptible plant. In this way, it is convenient to designate the cells containing active phytopathogens at the beginning of the propagation process. These inoculated cells are considered uniformly distributed and independent of the inoculated states of their neighbors. Then, using the Newman-Ziff algorithm, susceptible plants are added one by one. The clustering process between adjacent cells satisfies the following rules: (i) both sites are occupied with susceptible plants, or (ii) the neighboring site is inoculated. Although they are simple rules, the presence of the inoculated cells has a relevant impact on the formation of clusters, and thus on the percolation threshold. The simulation is stopped with the emergence of the spanning cluster of susceptible or diseased plants. The estimation of the percolation threshold is carried out by analyzing the generated data. Figure 6 shows the results of the percolation threshold as a function of the percentage of inoculated cells at the beginning of the propagation process for a plantation configured by square lattices with nearest and next-to-nearest neighbors, previously reported in Refs. [15,16].

In the context of this model, the *Phytophthora* propagation can only occur on susceptible plants, so the susceptibility takes the role of the occupation probability of traditional percolation lattices. Therefore, the percolation threshold is directly associated with the critical susceptibility χ_c of the plants. This means that the plantation should be sowed with plants having a susceptibility less than χ_c to avoid the outbreak. Similarly to the cases of square lattices with a fraction of extended neighbors, the critical susceptibility decreases as I grows. It is worth mentioning that there exists a minimal susceptible value that allows sowing the entire plantation even when all the cells are inoculated. However, considering that *Phytophthora* can survive under adverse environmental conditions, the management of the plantation is crucial in order to prevent outbreaks in future farming cycles.

We recall that this agroecological model connects sites over the regular neighborhood definition. However, the percolation threshold evolves similarly to square lattices with a fraction of extended neighbor sites. Here, the regular sites

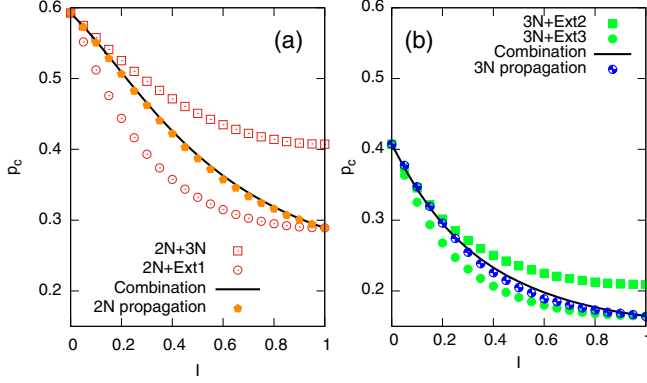


FIG. 6. Comparison between the percolation threshold of composite square lattices, the critical susceptibility of the agroecological model, and the linear combination approximation of Eqs. (9) and (10) (solid lines). (a) Case of 2N plantations. Squares and circles are the percolation thresholds of 2N+3N and 2N+Ext1 composite systems, respectively. Pentagons are the critical susceptibility of the agroecological model. (b) Case of 3N plantations. Squares and circles are the percolation thresholds of 3N+Ext2 and 3N+Ext3 composite systems, respectively. Semifilled circles are the critical susceptibility of the agroecological model.

correspond to the neighborhood definition used for clustering. Meanwhile, the extended sites must be determined by analyzing how the presence of the inoculated cells modifies the neighbor definition to connect susceptible plants, as depicted in Fig. 1. In what follows, we refer to 2N and 3N plantations as those sowed in a configuration based on 2N and 3N neighborhoods, respectively. Particularly for 2N and 3N plantations, we determine that the extended neighborhoods are 3N and Ext2 at low I -values but become Ext1 and Ext3 at high I -values, respectively.

Notice that the critical susceptibilities for 2N and 3N plantations are bounded as follows (see Fig. 6):

$$p_{c,2N+3N} \leq \chi_{2N} \leq p_{c,2N+Ext1},$$

$$p_{c,3N+Ext2} \leq \chi_{3N} \leq p_{c,3N+Ext3},$$

where $p_{c,reg+ext}$ denotes the percolation threshold for the combination of neighborhoods *reg* and *ext*. For the sake of notation, we indicate the critical susceptibility by χ . Moreover, we found that the critical susceptibilities can be well-reproduced by the following linear combinations:

$$\chi_{2N} = (1 - I)p_{c,2N+3N} + Ip_{c,2N+Ext1}, \quad (9)$$

$$\chi_{3N} = (1 - I)p_{c,3N+Ext2} + Ip_{c,3N+Ext3}. \quad (10)$$

Equations (9) and (10) are shown in Fig. 6 as solid lines. We also find an exponential behavior for the critical susceptibilities at low I values:

$$\chi_{2N} \propto 1 - \frac{I}{\lambda'_1} + O(I^2) \approx e^{-I/\lambda'_1}, \quad (11)$$

$$\chi_{3N} \propto 1 - \frac{I}{\lambda'_2} + O(I^2) \approx e^{-I/\lambda'_2}, \quad (12)$$

where

$$\lambda'_1 = \frac{\lambda_{2N+3N}}{1 - \frac{p_{c,3N}}{p_{c,2N}}} \quad \text{and} \quad \lambda'_2 = \frac{\lambda_{3N+Ext2}}{1 - \frac{p_{c,Ext2}}{p_{c,3N}}}. \quad (13)$$

By discussing the case of 2N plantations, we now illustrate the applicability of Eqs. (9) and (10). Equation (9) indicates that the combinations 2N+3N and 2N+Ext1 are picked with probabilities $1 - I$ and I , respectively. By construction, the regular and extended sites are also determined with probabilities $1 - I$ and I , respectively. All the possibilities combine to give the probabilities $1 - I$, $I(1 - I)$, and I^2 of the added site has vicinity 2N, 3N, and Ext1, respectively. In the limit of low I , the added sites in simulations are mostly 2N, with a few ones with the 3N vicinity. As I rises, the number of sites with extended neighborhoods takes place and the percolation threshold decreases. In the limit of high I , the system is mainly formed by Ext1 sites. At this point, the system becomes homogeneous, and the critical susceptibility approaches $p_{c,2N+Ext1}$. Using this framework, all the effects of inoculated cells are taken into account at once by incorporating sites with extended neighborhoods. Note that Eqs. (9) and (10) imply that composite systems discussed in this manuscript accurately describe the agroecology model in the limits $I = 0$ and 1. Nevertheless, this model resembles percolation systems comprising three neighbor definitions for intermediate I values. Therefore, agroecological applications can be described by a percolation system comprising more than two neighborhood definitions.

V. CONCLUSIONS

In this work, inspired by the problem of the propagation of *Phytophthora* zoospores on plantations, we introduced a percolation model on square lattices that includes sites with a combination of two different neighborhood definitions. In particular, we explore all possible pair combinations of five neighborhoods that extend beyond the next-to-nearest definition, which are depicted in Fig. 2. By using computational simulations, we estimate the percolation threshold for all those systems as a function of the fraction of sites with extended vicinity.

We found that the percolation threshold of systems with combined neighborhoods smoothly decreases from $p_{c,reg}$ to $p_{c,ext}$, which can be well-fitted by the q -Exponential function as seen in Eq. (4). In the limit of low values of the fraction of sites with the extended neighborhood, the percolation threshold exponentially decays with I , where the rate constant is the inverse of the scale (λ) of (4). Moreover, we related the q -Exponential parameters to the differences in the radius of gyration between the regular and extended neighborhoods. Explicitly, $\lambda \propto e^{-m(R_{g,ext} - R_{g,reg})}$ and $1/n \sim (R_{g,ext} - R_{g,reg})$. However, the latter relations may no longer be valid for combinations with very small differences in the radius of gyration, as in the case of the combination Ext2+Ext3, whose fitting parameters deviate from the trend of the other cases. Further analysis is required to corroborate this hypothesis for systems with neighborhoods extended beyond those discussed in this manuscript.

Additionally, we compared our estimations of the percolation threshold with the results reported for the critical susceptibility of monoculture plantations. In the context of the agroecological model, I corresponds to the fraction of inoculated cells at the beginning of the propagation process. Similar to the extended sites in the model presented in this

manuscript, these cells act as bridges that connect susceptible plants beyond the neighbor definition of the lattice that models the plantation when they are placed in empty cells or with a resistant plant. It is worth mentioning that the critical susceptibilities for 2N and 3N plantations are well-described by the linear combinations [see Eqs. (9) and (10)] of the percolation threshold of the composites 2N+3N and 2N+Ext1 and 3N+Ext2 and 3N+Ext3 (see Fig. 6), respectively. We also found that the critical susceptibility behaves as an exponential decay in the limit of low values of J . In Eq. (13) we report the decay constant for 2N and 3N plantations. Note that the agroecological model can also motivate the study of systems with more than two extended neighborhoods.

This work can be broadened in different directions. One possibility is to consider other regular lattices, for instance the triangular or the honeycomb. Analyzing the bond or the joint site-bond percolation model under this approach would

be meaningful. Another possibility consists of including the linear combination approach in more complex situations, for example in polyculture or structured plantations. It is worth noticing that all these perspectives are inspired by the agroecological model.

ACKNOWLEDGMENTS

This work was funded by Consejo Nacional de Humanidades, Ciencias y Tecnologías (CONAHCYT-México) under Project No. CF-2019/2042, graduated fellowships Grant No. 1140160, and postdoctoral fellowship Grant No. 289198. The authors thankfully acknowledge the computer resources, technical expertise, and support provided by the Laboratorio Nacional de Supercómputo del Sureste de México, CONAHCYT member of the network of national laboratories.

-
- [1] J. M. Hammersley, *Ann. Math. Stat.* **28**, 790 (1957).
 - [2] H. L. Frisch and J. M. Hammersley, *J. Soc. Ind. Appl. Math.* **11**, 894 (1963).
 - [3] D. Stauffer and A. Aharony, *Introduction To Percolation Theory* (Taylor & Francis, Philadelphia, 2003).
 - [4] A. L. Efros, *Physics And Geometry of Disorder* (Mir, Moscow, 1982).
 - [5] B. Bollobás and O. Riordan, *Percolation* (Cambridge University Press, Cambridge, 2006).
 - [6] J. W. Essam, *Rep. Prog. Phys.* **43**, 833 (1980).
 - [7] G. Grimmett, *What is Percolation?* (Springer, Berlin, 1999).
 - [8] M. Sahimi, *Applications of Percolation Theory* (Taylor & Francis, Boca Raton, FL, 1994).
 - [9] P. E. Seiden and L. S. Schulman, *Adv. Phys.* **39**, 1 (1990).
 - [10] J. C. Texca García, D. Rosales Herrera, J. E. Ramírez, A. Fernández Téllez, and C. Pajares, *Phys. Rev. D* **106**, L031503 (2022).
 - [11] J. E. Ramírez, B. Díaz, and C. Pajares, *Phys. Rev. D* **103**, 094029 (2021).
 - [12] J. E. Ramírez, D. Rosales Herrera, J. Velázquez-Castro, B. Díaz, M. I. Martínez, P. Vázquez Juárez, and A. Fernández Téllez, *Rev. Mex. Fis.* **68**, 011701 (2022).
 - [13] M. Pardo-Araujo, D. García-García, D. Alonso, and F. Bartumeus, *Sci. Rep.* **13**, 11409 (2023).
 - [14] J. E. Ramírez, E. Molina-Gayosso, J. Lozada-Lechuga, L. M. Flores-Rojas, M. I. Martínez, and A. Fernández Téllez, *Phys. Rev. E* **98**, 062409 (2018).
 - [15] J. E. Ramírez, C. Pajares, M. I. Martínez, R. Rodríguez Fernández, E. Molina-Gayosso, J. Lozada-Lechuga, and A. Fernández Téllez, *Phys. Rev. E* **101**, 032301 (2020).
 - [16] D. Rosales Herrera, J. E. Ramírez, M. I. Martínez, H. Cruz-Suárez, A. Fernández Téllez, J. F. López-Olguín, and A. Aragón García, *Chaos* **31**, 063105 (2021).
 - [17] I. Taguas, J. A. Capitán, and J. C. Nuño, *Phys. Rev. E* **105**, 064301 (2022).
 - [18] K. Lamour, *Phytophthora: A Global Perspective* (CAB International, Croydon, UK, 2013).
 - [19] O. K. Ribeiro, *Q. Rev. Biol.* **54**, 187 (1978).
 - [20] R. C. Ploetz and J. L. Haynes, *Proc. Fla. State Hort. Soc.* **113**, 211 (2000).
 - [21] A. R. Hardham, *Mol. Plant Path.* **6**, 589 (2005).
 - [22] W. E. Fry and S. B. Goodwin, *Plant Dis.* **81**, 1349 (1997).
 - [23] A. J. Gevens, R. S. Donahoo, K. H. Lamour, and M. K. Hausbeck, *Phytopathology* **97**, 421 (2007).
 - [24] M. E. J. Newman and R. M. Ziff, *Phys. Rev. Lett.* **85**, 4104 (2000).
 - [25] M. E. J. Newman and R. M. Ziff, *Phys. Rev. E* **64**, 016706 (2001).
 - [26] M. D. Rintoul and S. Torquato, *J. Phys. A* **30**, L585 (1997).
 - [27] A. Coniglio, *J. Phys. A* **15**, 3829 (1982).
 - [28] R. M. Ziff, *Phys. Rev. Lett.* **69**, 2670 (1992).
 - [29] K. Malarz and S. Galam, *Phys. Rev. E* **71**, 016125 (2005).
 - [30] M. Majewski and K. Malarz, *Acta. Phys. Pol. B* **38**, 2191 (2007).
 - [31] G. Wilk and Z. Włodarczyk, *Phys. Rev. Lett.* **84**, 2770 (2000).